

Tectonic Geomorphology and Paleoseismology of the Sharkhai fault: a new source of seismic hazard for Ulaanbaatar (Mongolia)

Abeer Al-Ashkar¹, Antoine Schlupp¹, Matthieu Ferry², Ulziibat Munkhuu³

¹Institut Terre et Environnement de Strasbourg, UMR 7063, Université de Strasbourg/EOST, CNRS ; 5 rue René Descartes, Strasbourg, 67084, France

²Géosciences Montpellier, Université de Montpellier - CNRS, Montpellier, France

³Institute of Astronomy and Geophysics, Mongolian Academy of Sciences, Ulaanbaatar, Mongolia

Correspondence to: Antoine Schlupp (antoine.schlupp@unistra.fr)

Abstract. We present [first](#) constraints from tectonic geomorphology and paleoseismology along the newly discovered Sharkhai fault near the capital city of Mongolia. Detailed observations from high-resolution Pleiades satellite images and field investigations allowed us to map the fault in detail, describe its geometry and segmentation, characterize its kinematics, and document its recent activity and seismic behavior (cumulative displacements and paleoseismicity). The Sharkhai fault displays a surface length of ~40 km with a slightly arcuate geometry, and a strike ranging from N42°E to N72°E. It affects numerous drainages that show left-lateral cumulative displacements reaching [94](#) m. Paleoseismic investigations document [faulting and depositional/erosional events](#) for the last ~3000 yr, and reveal that the [most recent event occurred between 775 CE and 1778 CE and the penultimate earthquake occurred between 1605 BCE and 835 BCE](#). The resulting time interval of [2496 ± 887 yr.](#) is the first constraint on the Sharkhai fault for large earthquakes. On the basis of our mapping of the surface rupture and the resulting segmentation analysis, we propose two possible scenarios for large earthquakes with likely magnitudes [of 6.7 ± 0.2 or 7.1 ± 0.7](#). Furthermore, we apply scaling laws to infer coseismic slip values and derive preliminary estimates of long-term slip rates. Finally, [these data help build a comprehensive model of active faults in that region and](#) should be [considered in](#) the seismic hazard assessment for the city of Ulaanbaatar.

Introduction and context

The tectonics of Mongolia are characterized by [the transition between the compressive structures associated with the India-Asia collision to the south, and the vast extensive structures of the Baikal Rift to the north](#) (Fig. 1). This induces [important complexity and variability expressed by dominantly strike-slip structures with minor thrust and normal faults](#) (Khilko et al., 1985; Cunningham, 2001; Ritz et al., 2003; Cunningham, 2007; Walker et al., 2008; Parfeevets and Sankov, 2012). In Central Mongolia, the Hangay dome [is surrounded by right- and left-lateral faults](#) (Cunningham et al., 1996; Schlupp, 1996; Bayasgalan, 1999; Bayasgalan et al., 1999a, Etchebes, 2011). [Western Mongolia is dominated by NW-SE-striking right-lateral and thrust faults distributed across the Mongolian Altai ranges, while southern Mongolia shows E-W left-lateral and thrust faults that produce the Gobi Altay restraining-](#)

- a supprimé: new
- a supprimé: 57
- a supprimé: the
- a supprimé: deposition record
- a supprimé: (PE) occurred between 1515 ± 90 BC and 945 ± 110 BC and the most recent event (MRE)
- a supprimé: after 860 ± 85 AD.
- a supprimé: 2080 ± 470 years
- a supprimé: between
- a supprimé: 4
- a supprimé: and
- a supprimé: 2
- a supprimé: between 0.2 ± 0.2 and 1.0 ± 0.5 mm/y.
- a supprimé: we propose that
- a supprimé: original observations and results from a newly discovered fault
- a supprimé: taken into account for
- a supprimé: and help build a comprehensive model of active faults in that region
- a supprimé: ¶
- a supprimé: a
- a supprimé: region
- a supprimé: numerous
- a supprimé: and uplift in west and central Mongolia
- a supprimé: displays several regional SW-NE extensive structures and
- a supprimé:
- a supprimé: ¶

63 bend topography. Finally, to the north the E-W Bolnay left-lateral strike-slip fault begins the transition with the
 64 Baikal rift system. The rate of deformation along faults in western and central Mongolia are relatively low with
 65 1.5 ± 0.26 to 3.8 ± 0.2 mm/yr, based on geological observations (Ritz et al., 2006; Etchebes, 2011; Rizza et al.,
 66 2015) and 2 ± 1.2 to 2.6 ± 0.5 mm/yr, based on geodetic data (Calais et al., 2003). Presently, the historical
 67 seismicity record in the region is short and poorly constrained (Khilko et al., 1985). Since 1905, seismicity has
 68 been highlighted by four great earthquakes with Mw ranging from 7.9 to 8.3-8.5 (9 and 23 July 1905, 11 August
 69 1931 and 4 December 1957) which occurred along the strike-slip faults of western and southwestern Mongolia
 70 (Fig. 1) with moderate background activity.

71 The region of Ulaanbaatar (capital of Mongolia) is situated in a folded system composed of Lower to Middle
 72 Carboniferous and Quaternary deposits (Tomurtogoo et al. 1998, Manandhar et al., 2016) (Fig.2). The
 73 Carboniferous formations are sandstone, mudstone, alternating beds of sandstone and mudstone with limited
 74 outcrops of conglomerate, siliceous mudstone, chert, felsic tuff and basalt (Takeuchi et al., 2013). Compared to
 75 western and southwestern Mongolia, the Ulaanbaatar region displays a different seismotectonic situation. Firstly,
 76 although several tectonic faults are clearly documented in the geological map (Fig. 2), their potential Quaternary
 77 activity remains unknown. Secondly, the level of recorded seismicity is significantly lower, in terms of both event
 78 frequency and magnitude (One century of seismicity in Mongolia map, 2000; Dugarmaa and Schlupp, 2000). The
 79 historical seismicity is poorly known and since 1957, when the instrumental period started, the activity has been
 80 limited to moderate earthquakes with magnitude less than 4.5 (Adiya, 2016). Nevertheless, several earthquakes
 81 were largely felt in Ulaanbaatar during the last century (Intensity MSK up to VI) without significant damage
 82 (Khilko et al., 1985). Regional deformation characterized by geodesy indicates 2-4 mm/yr. of E-SE horizontal
 83 displacement with respect to Eurasia (Miroshnichenko et al., 2018).

84 Between 2005 and 2019, more than ten swarm episodes of moderate earthquakes $M < 4.5$ have been recorded and
 85 accurately relocated ~ 10 km west of the capital (Adiya, 2016). Tectonic geomorphology investigations focused
 86 on the swarm area revealed evidence of Quaternary activity along the Emeelt fault (Ferry et al. 2010; Schlupp et
 87 al. 2010a; Ferry et al. 2012; Schlupp et al., 2012; Dujardin et al. 2014). This structure is located near the eastern
 88 end of the Hustai fault, strikes $N140^\circ$ (Fig. 2) and displays dominantly right-lateral kinematics with a reverse
 89 component. Recent studies suggest that it could produce earthquakes of Mw 6-7 (Schlupp et al., 2012). Located ~
 90 30 km west of Ulaanbaatar, the Hustai (alternative spelling Khustai) fault exhibits a remarkable morphology that
 91 displays recent markers affected by left-lateral and normal faulting, and is composed of several segments with a
 92 total length of 212 km. It is considered capable of producing earthquakes of M_x 6.5-7.5 (Ferry et al., 2010; Schlupp
 93 et al., 2010b; Fleury et al., 2011; Ferry et al., 2012). To the northeast of Ulaanbaatar, at ~ 15 km from the city
 94 center, the surface expression of the Gunj Fault is visible along ~ 20 km; it is oriented $N45^\circ$ and is evidenced by
 95 right-lateral displacements affecting gullies and reaching 25 m (Demberel et al., 2011), vertical scarps and flower
 96 structures (Imaev et al., 2012). Finally, the Ulaanbaatar Fault has been recently described by Suzuki et al. (2020):
 97 it displays scarps, pressure ridges and deformed Pleistocene deposits over a length of ~50 km. Preliminary results
 98 suggest the fault could produce earthquakes with Mw ranging from 6.5 to 7.1 depending on the rupture scenario
 99 (surface rupture length from 20 km to 50 km).

100 The most recent addition to the ongoing effort to document active faults within the intensely developing Greater
 101 Ulaanbaatar region was carried out to the south of the city, where the new international airport is built. There, we

a déplacé vers le bas [1]: poorly constrained (Khilko et al., 1985).

a supprimé: Presently, the knowledge of historical seismicity in the region is

a supprimé: Since 1905, the seismicity has been highlighted by four great earthquakes of $M_w > 8$ (9 and 23 July 1905, 11 August 1931 and 4 December 1957) which occurred along the strike-slip faults of western Mongolia (Fig. 1) and moderate background activity. ...he observed ...ate of deformation along the ...aults,...in western and central Mongolia, (... [1])

a déplacé (et inséré) [2] (... [2])

a déplacé vers le haut [2]: based on geodetic data (Calais et al., 2003).

a déplacé (et inséré) [3]

a supprimé: The situation differs around the capital Ulaanbaatar where the recorded seismicity is much lower...ompared to western and southwestern Mongolia, the Ulaanbaatar region displays a different seismotectonic situation. Firstly, although several tectonic faults are clearly documented in the geological map (Fig. 2), their potential Quaternary activity remains unknown. Secondly, the level of recorded seismicity is significantly lower, in terms of both event frequency and magnitude (One century of seismicity in Mongolia map, 2000; Dugarmaa and Schlupp, 2000). The historical seismicity is poorly known and since 1957, when the instrumental period started, the activity has been limited to moderate earthquakes with magnitude less than 4.5 (Adiya, 2016). Nevertheless, several earthquakes were largely felt in Ulaanbaatar during the last century (Intensity MSK up to VI) without significant damage. ... (Khilko et al., 1985). Regional deformation characterized by geodesy indicates 2-4 mm (... [3])

a supprimé: Since 2005, a stronger seismic activity ($M \leq 4.5$) has been observed...etween 2005 and 2019, more (... [4])

a déplacé (et inséré) [4]

a supprimé: Schlupp et al., 2010a), which prompted studies in tectonic geomorphology and paleoseismology to (... [5])

a supprimé: Emeelt fault: This fault has also been identified recently using tectonic geomorphology following a seis (... [6])

a déplacé vers le haut [4]: 2) and displays dominantly right-lateral kinematics with a reverse component.

a supprimé: Recent studies suggest that it could produce earthquakes of magnitude 6-7 (Ferry et al., 2010; Schlup (... [7])

a déplacé vers le haut [3]: of conglomerate, siliceous mudstone, chert, felsic tuff and basalt (Takeuchi et al., 2013).

a supprimé: In addition, Ulaanbaatar is located at the Tuul River Valley on a sedimentary basin of alluvial deposit (... [8])

a déplacé vers le bas [5]: (Odonbaatar 2011, Tumurbaatar et al., 2019).

a supprimé: Although the geological map (Fig. 3) displays several tectonic faults distributed in the Ulaanbaatar arc (... [9])

a déplacé vers le bas [6]: The growth of the capital is very important since the last two decades, the population in 1998

a supprimé: For example, in the city, new tall buildings have been erected and at 30 kilometers...as carried out (... [10])

a supprimé: ¶

449 combined the analysis of high-resolution satellite images and field investigations, and discovered two active faults
 450 hereafter called "Sharkhai fault" located ~ 35 km south of the capital and only 10 km south of the new airport and
 451 the "Avdar fault" (Fig. 2) (Al-Ashkar, 2015). In this study, we present a detailed characterization of the Sharkhai
 452 fault based on remote sensing analysis, geomorphological observations and paleoseismological investigations, and
 453 propose the first results pertaining to its Holocene activity, and associated characteristics (segmentation,
 454 kinematics, and paleoseismicity).

456 1 Morphotectonic description

457 1.1 Surface trace Mapping

458 1.1.1 Methodology

459 Considering the well-expressed geology (Carboniferous age) combined with slow active deformation rates, and
 460 low erosion and sedimentation rates (continental steppe context), our strategy consisted in mapping faults at high
 461 spatial resolution and characterizing their subtle cumulative expression within Quaternary deposits. To identify
 462 and quantify horizontal and vertical deformation we based our analysis on very high resolution orthorectified
 463 Pleiades satellites images (multispectral RGB-NIR at 2 m resolution and panchromatic at 0.5 m resolution,
 464 hereafter referred to as HR images) and high-resolution digital elevation models SRTM 1" at 30 m resolution and
 465 TanDEM-X at 12 m resolution, (hereafter referred to as DEM). Additional images from Google Earth acquired at
 466 different seasons provided complementary information. Remote sensing analysis was supplemented by field
 467 campaigns to verify, correct and complement these observations, perform detailed geomorphological mapping and
 468 excavate a paleoseismological trench.

469 1.1.2 Overview

470 Our observations show that the main trace of the Sharkhai fault, striking ENE-WSW, extends along 40 km (from
 471 A1 to A7 in Fig. 3). Along most of its length, the surface rupture corresponds to a documented geological structure
 472 (Fig. 2) that was not characterized as active in previous studies (Tomurtogoo et al., 1998). The main
 473 geomorphological features observed along the Sharkhai fault are offset drainages connected by faint lineaments
 474 that can be followed on HR images. In the field, they are locally expressed as smoothed scarps (less than 50 cm
 475 high) and break in slope and mark the eroded fault trace. Near the middle of the fault trace, a well-developed 1.4-
 476 km-wide extensional jog (Fig. 3, A3 and A4) accommodates a right step, which suggests that the fault can be
 477 segmented into two major sections: the southern section (strike N42 to N55) and the northern section (strike N55
 478 to N72) (Fig. 3 and 5). Below we describe the fault surface trace from the southwest to the northeast and detail the
 479 various features documenting recent activity and segmentation.

480 1.1.3 Southern section

481 Despite a generally weak morphological expression due to long-term erosion and, locally, recent stream deposits,
 482 the surface trace can be followed on HR images and confirmed by field observations (Fig. 4). The southern section

- a supprimé: we
- a supprimé: surface traces of
- a supprimé: we call
- a supprimé: and "Avdar fault", which shows clear evidence for a major seismic activity (Fig.
- a déplacé vers le bas [7]: 2) (Al-Ashkar, 2015).
- a supprimé: ¶
- Here, we present the Sharkhai fault
- a déplacé (et inséré) [7]
- a supprimé: . Along the Sharkhai fault, few moderate earthquakes ($M \leq 3.7$) were observed between 2004 and 2007. We present hereafter evidence of holocene activity,
- a supprimé: detailed mapping, kinematic, identification and dating of past earthquakes, recurrence time of large events
- a supprimé: combined very
- a supprimé: . and low
- a supprimé: .
- a supprimé: .
- a supprimé: background
- a supprimé: We
- a supprimé: (hereafter DEM;
- a supprimé:) to identify and quantify horizontal and vertical deformation. In addition, we used
- a supprimé: images for specific areas where multi-date data could complement Pleiades images.
- a supprimé: our
- a supprimé: 4). It is associated with eroded and smoothed surficial ruptures
- a supprimé: die off beyond the end points. We did
- a supprimé: observe any connection with other known
- a supprimé: structures. The Sharkhai fault does not fo... [11]
- a supprimé: ¶ ... [12]
- a supprimé: of 1.4 km width associated with a 13° cl... [13]
- a supprimé:). It
- a supprimé: Sharkhai
- a supprimé: subdivided
- a supprimé: south
- a supprimé: north
- a supprimé: 4). We observe in the field only an appar... [14]
- a supprimé: hereunder
- a supprimé: traces
- a supprimé: The south section runs for ~ 22 km betw... [15]
- a supprimé: geomorphologic
- a supprimé: . except some places where they cannot b... [16]
- a supprimé: or
- a supprimé: deposition
- a supprimé: ¶

545 runs for ~ 22 km from points A1 to A3 (Fig. 3) where the fault trace dies out at a large extensional step-over. The
 546 main geometric features that we detail hereafter are strike changes and step-overs.

a supprimé: local streams. ...oints A1 to A3 (Fig. 3) where the fault trace dies out at a large extensional step-over. The main geometric features that we detail here ... [17]

547 At its southern extremity, between points A1 and A2 the fault strikes N42° on average (Fig. 3, 4 and 5). Northward
 548 of A2, the average direction turns from about N42°E to N50°E, which is the largest strike variation along the
 549 southern section. In detail, we observe several small step-overs (3, 7 and 70 m width) and locally several changes
 550 in strike over short distances (a few hundred meters). Between A2 and B, the fault trace cuts through a
 551 Carboniferous hill (1450 to 1645 m elevation) and the top of two successive hills that are oriented N5° and N330°
 552 (Fig. 3 and 4). The fault displays an en-echelon geometry between B and C (Fig. 6) with secondary branches
 553 parallel or oblique to the main trace. Their lengths range from 190 m to 1.6 km and strike between N58° and N74°.
 554 Beyond, the fault continues through a valley floor covered with Quaternary alluvial deposits where the trace
 555 disappears. Along an 8-km-long section where the trace cuts hills and valleys, we identified six cumulative left-
 556 lateral offsets (Fig. 3 and Fig. 6). The first is a drainage shifted by 53 ± 6 m (P1 in Fig. 3 and Fig. 7). It corresponds
 557 to the maximum offset identified along the southern section of the Sharkhai fault (Table 1). The minimum offsets
 558 observed are 6.25 ± 1.65 m (P2 in Fig. 3 and Fig. 8) and 6.5 ± 1.5 m (P5 in Fig. 3 and Fig. 9). The three other
 559 cumulative offsets are 36 ± 5 m (P3 in Fig. 3 and Fig. A1), 30 ± 5 m (P4 in Fig. 3 and Fig. A2), and 36 ± 2 m (P6
 560 in Fig. 3 and Fig. A3). It should be noted that half of the documented offsets display similar values (30 m to 36
 561 m), which suggests they may have a common climatic origin (i.e. a Late Pleistocene humid period).

a supprimé: ...between locations...oints A1 and A2 (Fig. 4) the fault strikes N42°E...on average. There, from south to north, we observe several small step-overs with size between 3, 7 and 70 m width. The ... (Fig. 3, 4 and 5). Northward of the average direction of surface traces, at A2, ...turns from about N42°E to N50°E, which is the largest strike variation along the southern section. From A2, the surface traces cut a Carboniferous hill (1450 to 1645 m elevation). We observe...n detail, we observe several small step-overs (3, 7 and 70 m width) and locally several changes in strike over short distances.

562 1.1.4 Northern section

563 The northern section runs for ~ 22 km from point A4 to point A7 (Fig. 3). It has a slightly arched shape geometry:
 564 its strike turns from N55° to N63° and N72° (Fig. 5). In contrast with the southern section, it shows less in-strike
 565 segmentation (no clear step-overs) and more off-fault deformation (10-m-long to 1-km-long sub-parallel or oblique
 566 secondary branches). Locally we also observe changes in the main fault strike over a few hundred meters. This
 567 section affects mostly Quaternary deposits (Tomurtogoo et al., 1998) as the trace runs through an area of lower
 568 elevation (mainly < 1500 m) and the trace frequently disappears, which may suggest limited recent surface
 569 deformation. At the northern part of the section we measured 94 ± 3 m of left-lateral horizontal offset affecting a
 570 stream (P7 in Fig. 3 and Fig. A4), the only one identified along the northern Sharkhai section and the largest along
 571 the entire fault. The drainage pattern along the northern section is less complex than that along the southern section
 572 but also less developed or preserved, which limits the possible records of displacement. As it reaches the SE part
 573 of the Khoshigt Khondii basin where the new international airport of Ulaanbaatar is built (point A7 in Fig. 3), the
 574 trace of the Sharkhai fault cannot be observed anymore, neither on remote sensing data nor in the field. It terminates
 575 into fluvial plains covered by Quaternary sediments. Hence, the total surface rupture length of the Sharkhai fault
 576 could be underestimated by a few kilometers.

(a few hundred meters). Between A2 and B, the fault cuts...race cuts through a Carboniferous hill (1450 to 1645 m elevation) and the top of two successive hills that are oriented N5°... and N330°, where drainage P1 recorded 57 ± 2 m of cumulated left-lateral offset (Fig. 4, P1 and ... (Fig. 5). It corresponds to the maximum offset identified along the Sharkhai fault (Table 1). The minimum offset observed (Fig. 4, P2) is 6.25 ± 0.65 m left-lateral strike slip (Fig. 6). Four other left-lateral cumulative offsets are identified and measured at P3 = 36 ± 4 m (Fig. 7), P4 = 30 ± 3 m (Fig. 8), P5 = 6.5 ± 0.5 m (Fig. 9) and P6 = 36 ± 1 m (Fig. 10). Between B... and A3 (Fig. 4), the average strike of the fault is N47°. The fault is arranged in echelons...). The fault displays an en-echelon geometry between B and C (Fig. 11). Several... with secondary branches are observed...arallel or oblique to the fault...ain trace. Their lengths range between...rom 190 m and...o 1.6 km and strike between N E...58 and N 74° E...74. Beyond, the fault continues through a valley floor covered with Quaternary alluvial deposits where we lost locally its trace.

a supprimé: [18]

a supprimé: north...orthern section runs for ~ 22 km from point A4 (Fig. 4, A4) ...o point A7 (Fig. 4, A7) affecting ...). It has a slightly arched shape geometry; its strike turns from N55° to N63° and N72° (Fig. 5). In contrast with the southern section, it shows less in-strike segmentation (no clear step-overs) and more off-fault deformation (10-m-long to 1-km-long sub-parallel or oblique secondary branches). Locally we also observe changes in the main fault strike over a few hundred meters. This section affects mostly Quaternary surface ...eprints. Its ... (Tomurtogoo et al., 1998) as the trace runs into... through an area of lower elevation (mainly < 1500 m) than the south section (mainly > 1500 m). In many places, we lost the fault ...nd the trace when it crosses wide Quaternary deposits...requently disappears, which could...ay suggest limited recent surface deformation. At the northern part of the section we measured 94 ± 3 m of left-lateral horizontal offset affecting a stream (P7 in Fig. 3 and Fig. A4), the only one identified along the northern Sharkhai section and the largest along the entire fault. The drainage pattern along the north...orthern section is less complex than (... [19]

a supprimé: [19]

a déplacé (et inséré) [8]

a déplacé vers le haut [8]: lateral offsets measured on the Sharkhai fault. Drainage name

a supprimé: Horizontal offset (m) ... [20]

a supprimé: [20]

577 Table 1: Summary of cumulative left-lateral offsets measured on the Sharkhai fault.

Drainage name	P1	P2	P3	P4	P5	P6	P7
Horizontal offset (m)	53 ± 6	6.25 ± 1.65	36 ± 5	30 ± 5	6.5 ± 1.5	36 ± 2	94 ± 3
Location (E/N m)	606481/ 5253332	606811/ 5253578	607399/ 5254010	608673/ 5254831	609209/ 5255368	609948/ 5256066	630457/ 5269135

822

823 2 Fault segmentation

824 Possible rupture scenarios and associated magnitudes along the Sharkhai fault are key parameters for estimating
 825 seismic hazard levels onto the city of Ulaanbaatar and the new airport. With limited information about historical
 826 seismicity along the fault, we may estimate the magnitude of possible events in relation to the length of the rupture
 827 (Wells and Coppersmith, 1994; Leonard, 2014). We use the identified discontinuities along the fault to discuss
 828 whether the fault should be divided into several segments (Fig. 5) that could break independently or not.

829 Step-overs, secondary branches, and fault strike changes can play an important role in the propagation of a rupture
 830 (nucleation and barrier) and consequently in the size of expected earthquakes (Poliakov et al., 2002; Wesnousky,
 831 2006; Klinger, 2010; Finzi and Langer, 2012; Biasi and Wesnousky, 2016; Biasi and Wesnousky, 2017). Usually,
 832 only kilometer-scale discontinuities are considered for the segmentation (Crone and Hailer, 1991; De Polo et al.,
 833 1991; Harris et al., 1991; Wesnousky, 2006; Wesnousky, 2008; Carpenter et al., 2012). Therefore, only the central
 834 step-over appears wide enough to separate the fault into two segments, southern and northern. The width of the
 835 other step-overs is much more limited, between 3 and 173 m, and is not clearly expressed in the geomorphology.
 836 Thus, we do not consider them as segment boundaries. Similarly, it has been proposed that changes in strike of
 837 more than 5° could play a role in fault segmentation (Lettis et al., 2002; Harris et al., 1991, Wesnousky, 2006;
 838 Finzi and Langer, 2012). Nevertheless, recent large earthquakes in Mongolia have shown that even larger changes
 839 in orientation had no impact on the segmentation [Mogod 1967 January 5 Mw 7.1 (Bayasgalan and Jackson,
 840 1999b); Bogd 1957 December 4 Mw 8 (Rizza et al., 2011)]. Along the Sharkhai fault, the changes in the orientation
 841 are either very local variation or of value not exceeding 9°. Thus, they are not considered as likely segment
 842 boundaries.

843 In conclusion, we propose two possible scenarios for large earthquakes on the Sharkhai fault depending on the
 844 role that the central step-over may play in the propagation of the rupture. The first scenario is that the entire fault
 845 (40 km) breaks during one earthquake. The second scenario is that the southern segment and the northern segment
 846 (22 km each) break independently.

847

848

849 3 Paleoseismic Investigations

850 To retrieve the chronology of surface-rupturing paleoearthquakes, we conducted the first paleoseismological study
 851 along the Sharkhai Fault at a site called Muka (Fig. 3 and J0). This site was selected based on geomorphological
 852 observations performed from high-resolution Pleiades satellite images, high-resolution TanDEM-X DEM and field
 853 surveys. Considering a priori slow rate of deformation, our strategy was to avoid apparently recent deposits found
 854 in wide alluvial valleys, as well as associated erosion processes, that could cover the recent deformation in the last
 855 3-4 meters or erode last event records and rather target relatively slow deposition processes such as colluvium on
 856 gentle slopes and abandoned or intermittent drainages. The subtle geomorphological expression of the Sharkhai
 857 fault combined with high elevation along most of its trace yielded only a few favorable sites where the fault is well
 858 expressed and potentially datable deposits are expected. The Muka site is located near the Zuummod - Buren Road

a supprimé: Without
 a supprimé: the

a supprimé:
 a supprimé:
 a supprimé:
 a supprimé: taken into account
 a supprimé: ,
 a supprimé: south
 a supprimé: north
 a supprimé: are
 a supprimé: three
 a supprimé: are
 a supprimé: ¶
 a supprimé:), but
 a supprimé: for

a supprimé: (Fig. 13)

a supprimé: south
 a supprimé: north

a supprimé: 4
 a supprimé: 14

a supprimé: (
 a supprimé:)

a supprimé: topography

a supprimé: ¶

882 and ~ 10 km SW of the new airport. There, the trace of the fault is clear, enhanced by a small scarp (about 30 cm
 883 high) (Fig. 10 c) and a striking difference in vegetation type and color, often indicative of a local contrast in
 884 lithology and/or hydrology in the shallow sub-surface. This small scarp suggests surface deformation with an
 885 apparent vertical offset that could be induced by horizontal slip along slopes. The fault affects here surface
 886 colluvium deposited along the flank of a small valley. Local gullies are intermittent and probably only active
 887 during important rainfall (Fig. 10A and B). Hence, we consider this site favorable to the accumulation of deposits,
 888 the preservation of the fault's paleoseismic history and to the determination of paleoearthquakes chronology by
 889 radiocarbon and/or OSL approaches.

- a supprimé: (< 50
- a supprimé: 14
- a supprimé:), which suggests apparent vertical deformation,
- a supprimé: The fault affects

890 The Muka site is located at 628253 m E/ 5268367m N along a straight section of the fault where deformation at
 891 the surface appears well-localized (Fig. 10). There, the fault marks a break in slope with a ~30-cm-high scarp and
 892 is crossed by short (100-500 m in length) shallow gullies. We excavated two trenches called Muka-K and Muka-
 893 L (Fig. 10B) ~150 m apart. Both trenches were ~20 m long, 1 m wide and up to 3 m deep as limited by the local
 894 permafrost. Heavy rainfall and thawing of the exposed permafrost destabilized overnight the fine deposits (silt and
 895 sand) found in Muka-K. Wide sections of the trench collapsed and the exposure was considered unsafe to work
 896 on. Stable substratum crops out at the bottom of Muka-L, which stabilized the whole section and gave time to
 897 reinforce the walls with wooden shores. In the following, we present the Muka-L exposure only.

- a supprimé: .
- a supprimé: suitable to preserve
- a supprimé: help determine its timing

898

899 3.1 Trench Stratigraphy

900 Both trench walls were cleaned, gridded, photographed and logged in detail. The Photomosaic of the trench (west
 901 and east wall), 15 m long and 3m deep, is built using 210 photographs. Since both walls yield similar information
 902 in terms of paleoseismicity, we only present the west wall in detail along with close-ups of the east wall for
 903 illustration (Fig. 11). In the following, we describe the stratigraphy, provide age constraints on the basis of
 904 radiocarbon-dated sediment samples and analyze abutting relationships to decipher the chronology of surface-
 905 rupturing earthquakes at this site.

- a supprimé:
- a supprimé: 14
- a supprimé: 14 b
- a supprimé: overnight
- a supprimé: Here
- a supprimé: and discuss

906 The base unit visible along the whole trench is composed of massive Carboniferous bedrock (U70). The U70
 907 exhibits widespread fracturation, localized shear zones with thin gouge development (< 2 cm). The uppermost 10-
 908 50 cm of U70 are composed of deeply weathered, well-sorted unstratified fine clasts (< 3 cm) that we interpret as
 909 the product of gelifraction. Numerous thin shear zones marked by whitish-to-yellowish clay cut through the whole
 910 unit and stop at its top surface. They generally exhibit a relatively steep dip to the south and produce duplexing
 911 features within the weathered part of U70. The top surface is very rough with deep troughs and systematically
 912 truncates reverse-geometry shear zones; it is interpreted as a well-developed erosion surface. Although the bottom
 913 of the trench was still frozen during the excavation done in summer, we didn't find clear indication of gelifraction
 914 of the erosional surface at top of U70.

- a supprimé: , gridded
- a supprimé:) is
- a supprimé: it
- a supprimé: constructed
- a supprimé: the
- a supprimé: 15
- a supprimé: analyse
- a supprimé:) that
- a supprimé:

915 Over the northern section of the trench, U70 is overlain with a ~1-m-thick unit of massive clast-supported coarse
 916 gravels and pebbles (U60). Clasts present the same lithology as U70, are very angular and well-stratified, which
 917 suggests they have been transported by water but only over a very short distance. U60 contains a few lenses of
 918 dark brown to black fine sand. Combining with the geometry of the lower erosion surface, we interpret U60 as a

- a supprimé: -
- a supprimé: -
- a déplacé (et inséré) [9]
- a supprimé: ¶

943 channel fill. Sample W3-S03 (Fig. 11g and Table 2) was collected within this unit and yields a radiocarbon
 944 calibrated age 1515 ± 90 BCE (3220 ± 30 BP).

945 Table 2: Radiocarbon dating of bulk-sediment samples collected in the Muka-L trench and dated by the Poznań Radiocarbon
 946 Laboratory. The software OxCal V2.4 (Ramsey, 2013) with 2-sigma error was used to obtain the calendric ages with Intcal13
 947 calibration curve (Reimer et al., 2013).

Sample name	Laboratory N.	Radiocarbon age (yr. BP)	Calibrated date (2-sigma)	Delta 13 (AMS)
Muka-L-W3-S03	Poz-56959	3220 ± 30	1515 ± 90 BCE	-24.5 ± 0.4
Muka-L-W3-S04	Poz-56961	2745 ± 30	945 ± 110 BCE	-27.4 ± 0.2
Muka-L-W4-S02	Poz-56958	2360 ± 30	450 ± 70 BCE	-35 ± 3.7
Muka-L-W2-S06	Poz-56963	1180 ± 25	860 ± 85 CE	-22.5 ± 0.7
Muka-L-W2-S05	Poz-56962	1950 ± 30	45 ± 80 CE	-24.2 ± 0.2

948
 949 In the central part of the trench, U70 is overlain by a ~8-m-wide, 50-cm-thick unit that pinches out at both tips
 950 (U50). This lens contains similar clasts then in U60 with a much smaller matrix fraction (clast-supported to
 951 openwork). It exhibits well-defined sub-horizontal stratigraphy and is interpreted as a low-energy channel.
 952

953 The southern half of U50 is itself overlain by a 5-10-cm-thick well-sorted fine sand unit (U40) that changes
 954 laterally to massive clay, locally grey but with widespread secondary oxidation. It fills a small basin bounded by
 955 U70 at the southernmost end of the trench. There, U40 displays growth strata and contains massive clay with rare
 956 scattered angular gravels (Fig. 11a). This marks a change in the depositional environment: a small pond in a rather
 957 dry climate with occasional clasts from the surrounding slope.

958 A higher well-developed layer (U30) crops out over the whole length of the trench. Unit 30 is composed of massive
 959 red clay and coarse sand with abundant scattered gravel and some well-sorted grey sand lenses (Fig. 11a). The
 960 clay fraction is dominant within the small depression (between $x=0$ and $x=4$ m) to the south and diminishes to the
 961 north where sand lenses are thicker (5-8 cm) and more continuous. There, the matrix contains numerous pockets
 962 of secondary white clay (Fig. 11b). Overall, the stratigraphic facies of U30 resemble red clay formations generally
 963 associated with a warm and humid climate (Feng et al., 2007).

964 Between $x = 9$ m and $x = 12$ m, three blocks with well-defined edges make up unit U20 composed of well-stratified
 965 sand and angular fine gravel with very little matrix resembling channel fill unit U50. It is considered allochthonous
 966 with respect to the rest of the stratigraphic section and interpreted as a small channel that flowed oblique to the
 967 fault. A modern equivalent could be seen in the shallow intermittent stream that flows across the site next to trench
 968 Muka-K (Fig. 11 b). We collected two samples from the top of U20: W2-S04 yielded a calibrated date 945 ± 110
 969 BCE (2745 ± 30 yr. BP) and W2-S05 a calibrated date 45 ± 80 CE (1950 ± 30 yr. BP). Since samples are both
 970 bulk sediments, the significant age difference may not be attributed to reworking of W2-S04. Furthermore, the age
 971 of W2-S05 sits very close to a rupture and exhibits dense live rootlets that could have been a guide for

a déplacé vers le haut [9]: U60 contains a few lenses of dark brown to black fine sand.

a supprimé: 15g...1g and Table 2) was collected within such a lens...his unit and yields a radiocarbon age of 3220 ± 30 yr BP ...alibrated to...ge 1515 ± 90 BC. (... [21])

a supprimé: from...n the Muka-L trench...and dated by the Poznań Radiocarbon Laboratory. The software OxCal V2.4 (Ramsey, 2013) with 2...sigma error was used to obtain the calendric ages with Intcal13 calibration curve (Reimer et al., 2013). (... [22])

a supprimé: Stratigraphic unit

Cellules insérées

a supprimé: W2-S06

a supprimé: U11 (mid-section)

a supprimé: 1180 ± 25

a supprimé: 860 ± 85 AD

a supprimé: W4-S02

a supprimé: U11 (base)

a supprimé: 2360

a supprimé: 450 ± 70 BC

a supprimé: W2-S05

a supprimé: U20

a supprimé: 1950

a supprimé: 45 ± 80 AD

a supprimé: W3-S04

a supprimé: U20

a supprimé: 2745 ± 30

a supprimé: 945 ± 110 BC

a supprimé: W3-S03

a supprimé: U60

a supprimé: 3220

a supprimé: 1515 ± 90 BC

a supprimé: Over

a supprimé: southern section...entral part of the trench, U70 is overlain by a ~8-m-wide, 50-cm-thick unit that pinches out at both tips (U50). This latter unit...ens contains similar clasts (in nature and size) to what is observed...hen in U60 with a much smaller matrix fraction (clast-supported to openwork). It exhibits well-defined sub-horizontal stratigraphy and is interpreted as a low (... [23])

a supprimé: third...alf of U50 is itself overlain with...y a 5-10-cm-thick well-sorted fine sand unit (U40) that changes laterally to massive clay, locally grey clay...ut with widespread secondary oxidation as it enters... It fills a small basin formed...ounded by the top of...U70 at the end of the trench. There, U40 displays growth strata and contains massive clay with rare scattered angular gravels (Fig. 15a...1a). This marks a different (... [24])

a supprimé: 15a...1a). The clay fraction is dominant (... [25])

a supprimé: 15...1 b). We collected two samples from (... [26])

a supprimé: [

1095 [contamination](#). Hence, we interpret W2-S05 as contaminated and rejuvenated with respect to its stratigraphic
1096 position and discard it from our analysis.

1097 Finally, the uppermost unit called U11 is a 0.8-to-1.5-m-thick massive fine sand and silt layer. It is overall grey in
1098 color, darker near its base and displays discontinuous brown to black lenses throughout the section. At the southern
1099 end of the trench, it contains clasts of U30, which indicates the base of U11 is an erosion surface. Above this local
1100 transition, no internal stratigraphy could be observed. Its top is dominated by weak present-day soil development
1101 (U10), which is only visible within the first 8-10 cm from the ground surface. We collected two sediment samples
1102 from U11 within dark lenses: one at the bottom (sample W4-S02) yielded [a calibrated date 450 ± 70 BCE \(2360](#)
1103 [± 30 yr. BP\)](#) and one in the mid-section (sample W2-S06) [with a calibrated date 860 ± 85 CE \(1180 ± 25 yr. BP\)](#).
1104 This is the youngest age constraint found in the Muka-L trench.

a supprimé: an age of 2360 ± 30 yr BP (
a supprimé: BC
a supprimé: an age of 1180 ± 25 yr BP (
a supprimé: AD

1106 [3.2 Surface faulting events at the Muka-L site](#)

1107 Trench Muka-L revealed numerous deformation features (Fig. [11a-e](#)): [interrupted and offset layers displaying step-](#)
1108 [like geometry \(Fig. 11a\), splays structures \(Fig. 11b\), and grabens \(between 6 m and 7 m in Fig. 11g\), among](#)
1109 others.

a supprimé: 3.2 Chronology of past surface-rupturing
earthquakes
a supprimé: 15a
a supprimé: 15a), flower
a supprimé: 15b
a supprimé: 15g
a supprimé: with
a supprimé: containing
a supprimé: 15f

1110 The Carboniferous bedrock (U70) is intensely deformed [by](#) widespread fractures and numerous shear zones
1111 dipping 30°-50° to the south and [infiltrated by](#) white to yellow clay. This unit is brittle enough for groundhogs to
1112 be able to dig through it (see the large burrow at x = 8 m in Fig. [11f-g](#)). This deformation is inconsistent with
1113 ruptures observed in upper units and is limited to U70; it is therefore considered representative of an ancient
1114 tectonic regime and will not be described any further here.

1115 The sedimentary section (units U60 to U10) is affected by ruptures exhibiting generally near-vertical dips with
1116 some dipping slightly to the south and a few to the north. [Splays with geometries resembling flower](#) and double
1117 flower structures (Fig. [11 b-c](#) and [Fig. 11g](#) at x=4.5 m) are the cross-section expressions of horizontal movement
1118 along [en-echelon](#) fissures and indicate a [strike-slip](#) component. This is confirmed by significant variations in unit
1119 thickness across faults as displayed by U60 between x=9 m and 12 m. Furthermore, numerous extensional features
1120 such as stepping ruptures at the edge of the pond, a graben at x=6-6.5 m and the collapse of the [completely](#)
1121 sedimentary section between x=10.5 m and 12 m [suggest](#) transensional [deformation](#). The detailed trench log (Fig.
1122 [11 g](#)) reveals that normal geometry ruptures are dominant south of x=8 m (main burrow) and expressed as
1123 distributed minor vertical individual offsets of 5-15 cm (with a possible contribution from strike-slip
1124 displacement). Dominantly strike-slip deformation appears to be limited to a narrow band between x=9 and 12 m.
1125 There, large vertical apparent displacements (> 50 cm) and allochthonous blocks suggest significant horizontal
1126 deformation.

a supprimé: Flower
a supprimé: 15
a supprimé:)
a supprimé: 14g
a supprimé:
a supprimé: strong
a supprimé: whole
a supprimé: indicate deformation is
a supprimé: , thus reflecting geomorphological observations.
a supprimé: 15
a supprimé: m

1127 Logged ruptures display [terminations at different levels](#). Between x=5m and 7.5 m all ruptures terminate at the top
1128 of U30 and are truncated by the upper erosion surface. A few more ruptures between x=8 m and 9 m appear to
1129 display a similar geometry, though extensive burrowing hinders proper observations. These ruptures would have
1130 affected the stratigraphy posterior to the deposition of U30 and prior to the erosion of its top surface; i.e. between

a supprimé: varying
a supprimé: .
a supprimé: 0 m and 3 m and between 5 m

a supprimé: ¶

1158 1605 BCE (upper bound of Muka-L-W3-S03) and 835 BCE (lower bound of Muka-L-W3-S0). A second
 1159 generation of ruptures cuts through the whole section and affects U11 and possibly U10 (soil development renders
 1160 our observations inconclusive): between $x=3$ m and 5 m, at $x=7$ m and between $x=9$ and 12 m. The event occurred
 1161 posterior to the deposition of the youngest unit (U11), i.e. It should be noted that a few isolated ruptures located at
 1162 around $x=3$ m and $x=6$ m affect the upper erosion surface (top of U30) but do not appear to propagate further
 1163 upward. Although they could be associated with an intermediate event, we propose they are associated with the
 1164 most recent one and their upward continuation could not be observed due to the lack of clear stratigraphy within
 1165 U11. Furthermore, small vertical offsets affect the top of U30 between $x=3$ and 5 m with an apparent component
 1166 (the bottom and top of U30 do not display the same offsets).

- a supprimé: 1515 ± 90 BC
- a supprimé: 945 ± 110 BC.
- a supprimé: m
- a supprimé: since 860 ± 85 AD.
- a supprimé: the edge of the pond (
- a supprimé: 3
- a supprimé:)
- a supprimé: m

1167 In summary, the Muka-L trench documents the erosion and deposition record for the last ~3000 yr, with varying
 1168 environments. Abutting relationships reveal at least two deformation events: (1) a most recent event (MRE) after
 1169 775 CE (lower bound of W2-S06). Considering that Ulaanbaatar was installed in 1778 (e.g. Majer and Teleki,
 1170 2006), a large earthquake after this date along this fault would have been reported in the historical documentation
 1171 which is not the case. Thus, the MRE occurred anytime between 775 CE and 1778 CE. (2) a penultimate event
 1172 (PE) occurred between 1605 BCE (upper bound of Muka-L-W3-S03) and 775 BCE (lower bound of Muka-L-W3-
 1173 S6).

- a supprimé: a penultimate event (PE) at 1605-775 BC and
- a supprimé: AD.

1175 4 Discussion and Conclusions

1176 4.1 Surface trace geometry and Inter-event time

1177 From our morphotectonic analysis based on field observations and HR remote sensing data, we mapped the
 1178 Sharkhai fault, oriented $N57^\circ (\pm 15^\circ)$, over a length of ~ 40 km (Fig. 5). The tips of the surface rupture terminate
 1179 into wide fluvial plains (a few km wide) where they are covered by sediments. Hence, the total surface rupture
 1180 length of the Sharkhai fault could be underestimated by a few kilometers. The surface expression of the fault is
 1181 divided into two main segments displaying a slightly arcuate shape and separated by a large extensional step-over
 1182 of 1.4 km in width. Both segments are of similar length (~ 22 km) with a lateral overlap of ~ 4 km. We also
 1183 describe internal geometric discontinuities that are typical for large strike slip faults: strike changes of 5° to 9° ,
 1184 local step-overs of 3 m to 173 m in width; secondary branches of 10 m to 1.6 km in length (Fig. 5 and 6). Generally,
 1185 these discontinuities are too small to play an important role in the rupture propagation and total length and related
 1186 earthquake size (Poliakov et al., 2002). Conversely, the width of the main extensional step-over corresponds to
 1187 features that may equally stop or promote the propagation of the rupture in similar settings (Wesnousky, 2006).

- a supprimé: about
- a supprimé: 13
- a supprimé: up to 10 km
- a supprimé: , about
- a supprimé: ,
- a supprimé: about
- a supprimé: described
- a supprimé: ° (from south to north $N42^\circ$, $N50^\circ$, $N55^\circ$, $N63^\circ$ and $N72^\circ$);...
- a supprimé: mainly at the northern end
- a supprimé: The
- a supprimé: 8
- a supprimé: 57
- a supprimé: .
- a supprimé: some

1188 Along strike, we documented 7 streams affected by left-lateral cumulative offsets ranging from 6.25 m to 94 m,
 1189 with two of about 6 m and three of 30-36 m (Fig. 3 and table 1). We did not observe systematic vertical
 1190 deformation; the local vertical displacements being easily explained as apparent and induced by horizontal slip
 1191 along slopes.

- a supprimé: Furthermore, our paleoseismic investigations reveal two paleoearthquakes
- a supprimé: fault: the penultimate earthquake (PE) occurred between 1515 ± 90 BC and 945 ± 110 BC and the most recent event (MRE) occurred after 860 ± 85 AD, which yields an inter-event time of 2080 ± 470 yr (between 1610 and 2550 yr)....

1192 Our work is the first paleoseismological study along the Sharkhai Fault. The Muka trench site is located near the
 1193 end of the mapped rupture (Fig. 3), which is not the standard strategy for such a study since deformation may be

- a déplacé vers le bas [10]: This is the first inter-event time constraint for the Sharkhai fault and it is comparable to values derived for major active faults elsewhere in Mongolia (e.g. Prentice et al., 2002; Rizza et al., 2015).
- a supprimé: 4
- a supprimé:]

1231 weakly expressed and the resulting record may be less legible and possibly incomplete. However, potential sites
 1232 are scarce along the Sharkhai Fault and this site was selected on the basis of remote sensing and field observations
 1233 for its relatively high sedimentary potential. It delivered well-expressed surface deformation and adequate deposits
 1234 for age determinations. The Muka-L trench analysis reveals two paleoearthquakes along the Sharkhai fault: the
 1235 most recent event (MRE) occurred between 775 CE and 1778 CE and the penultimate earthquake (PE) occurred
 1236 between 1605 BCE and 775 BCE, which yields an inter-event time of 2496 ± 887 yr. (between 3383 yr. and 1610
 1237 yr.). This is the first inter-event time constraint for the Sharkhai fault and it is comparable to values derived for
 1238 major active faults elsewhere in Mongolia (e.g. Prentice et al., 2002; Rizza et al., 2015).

a supprimé: partial. Potential
 a supprimé: nevertheless

1239 **4.2 Magnitude, co-seismic displacement and slip rates**

1240 The data collected on the Sharkhai fault, although preliminary, allow us to make some considerations on the
 1241 seismic potential of this fault. Based on the fault geometry and internal organization we may consider two rupture
 1242 scenarios: i) the entire fault ruptures into a single event over a length of 40 km, and ii) the two segments rupture
 1243 independently into two distinct events over lengths of 20 km (Table 3). In the absence of coseismic slip observed
 1244 along the fault, we used the scaling laws of Wells and Coppersmith, 1994 and more recent work done by Leonard,
 1245 2014 to associate magnitudes and co-seismic slip values to each scenario based on the length of the activated
 1246 segments. We used the regression to estimate magnitude (M) according to surface rupture length (SRL), and the
 1247 regression between co-seismic slip or average displacement (AD) according to surface rupture length (SRL).

a supprimé: ¶
 a supprimé: Finally,
 a supprimé: four
 a supprimé: , ii) same as previous with an extended length of 50 km to account for underestimation, iii
 a supprimé: , and iv) same as previous with extended lengths of 25 km to account for underestimation
 a supprimé: Considering
 a supprimé: proposed by
 a supprimé: (
 a supprimé: - named hereafter WC94)
 a supprimé: (
 a supprimé: - named hereafter L14), we can
 a supprimé: .

1248 For magnitude: $M = a + b * \log(SRL)$

1249 Wells and Coppersmith (1994) give for strike slip faults: $a = 5.16 \pm 0.13$ and $b = 1.12 \pm 0.08$.

1250 Leonard (2014) gives for strike slip faults: $a = 4.17$ (3.77 to 5.55), $b = 1.667$

1251 For average co-seismic slip: $\log(AD) = a + b * \log(SRL)$

1252 Wells and Coppersmith (1994) give for strike slip faults: $a = -1.70 \pm 0.23$ and $b = 1.04 \pm 0.13$.

1253 Leonard (2014) gives for strike slip faults with SRL 3.4 to 40 km: $a = -3.844$ (-4.30 to -3.40), $b = 0.833$

1254 The deduced magnitudes M_w are 6.7 ± 0.2 and 7.1 ± 0.7 for the two segments and entire fault scenarios respectively
 1255 (table 3). It is important to notice that we did not observe a single co-seismic offset in the field. Therefore, the co-
 1256 seismic slip values are estimates based on the length of the rupture, considering the two scenarios, and Wells and
 1257 Coppersmith (1994) or Leonard (2014) relations (see relations above). The deduced co-seismic slip estimates vary
 1258 between 0.65 ± 0.5 m and 1.3 ± 0.9 m (table 3).

a supprimé: vary between
 a supprimé: 4
 a supprimé: 2 and the
 a supprimé: 6
 a supprimé: 6 ± 1.2
 a supprimé: For the scenario when the entire fault breaks in one event, the slip rate is between 0.5 ± 0.3 and 0.9 ± 0.5 mm/yr; for the scenario when the two segments break separately, it is between 0.3 ± 0.3 and 0.4 ± 0.3 mm/yr (Table 4)....

1259

1260

1261

1262

1263

a supprimé: ¶

1290

1291 **Table 3:** Estimation of the magnitude and average co-seismic slip using Wells and Coppersmith (1994) and Leonard (2014)
 1292 regressions. The fault length is determined from the segmentation scenarios.

Segmentation scenario	Rupture length (km)	Magnitude (Mw)		Average co-seismic slip (m)	
		Wells and Coppersmith, 1994	Leonard, 2014	Wells and Coppersmith, 1994	Leonard, 2014
Entire fault	40	6.95 ± 0.2	7.1 ± 0.7	1.3 ± 0.9	1.3 ± 0.9
2 segments	22	6.7 ± 0.2	6.7 ± 0.7	0.65 ± 0.5	0.8 ± 0.5

1293

1294 For the scenario when the entire fault breaks in one event, the slip rate is between 0.4 ± 0.3 and 0.8 ± 0.6 mm/ yr.
 1295 and for the scenario when the two segments break separately, it is between 0.2 ± 0.1 and 0.5 ± 0.2 mm/ yr. (Table
 1296 4).

1297 Table 4: Minimum and maximum inter-event time and slip rate for the Sharkhai fault (WC94: Wells and Coppersmith, 1994;
 1298 L14: Leonard, 2014).

Segmentation scenario	Co-seismic offset (m)	Inter-event time (years) Min / Max	Slip rate (mm/year)
			Max / Min
Entire fault	1.3 ± 0.9 (WC94 and L14)	1610 / 3383	0.8 ± 0.6 / 0.4 ± 0.3 (WC94 and L14)
2 segments (South and North)	0.6 ± 0.5 (WC94)	1610 / 3383	0.4 ± 0.2 / 0.2 ± 0.1 0.3 (-0.2 + 0.3) (WC94)
	0.8 ± 0.5 (L14)		0.4 ± 0.2 / 0.2 ± 0.1 0.3 (-0.2 + 0.3) (L14)
2 segments (South and North)	0.65 ± 0.5 (WC94)	1610 / 3383	0.4 ± 0.2 / 0.2 ± 0.1 (WC94)
	0.8 ± 0.5 (L14)		0.5 ± 0.2 / 0.2 ± 0.1 (L14)

1299

1300 The timing of the last event (between 775 CE and 1778 CE), the inter-event time (between 1610 and 3383 yr) and
 1301 the slip rate (between 0.2 ± 0.1 and 0.8 ± 0.6 mm/ yr) are consistent with the weakly expressed morphology of
 1302 the fault. Notice that considering the uncertainties, the lowest slip rate value could be as low as ≈ 0.1 mm/ yr with
 1303 the scenario of an event breaking only one segment of the Sharkhai fault every 3383 yr on average. The upper
 1304 bound (0.8 ± 0.6 mm/ yr) appears unrealistically high for a single structure concerning region-wide values.

a supprimé:
 a supprimé: 9
 a supprimé: 6.9...1 ± 0.2 (... [27])
 a supprimé: ± 0.4
 a supprimé: 4... ± 0.2 (... [28])
 a supprimé: 6
 a supprimé: 6... ± 0.4 (... [29])
 a supprimé: Entire Fault (observed + 10 km) (... [30])
 a supprimé: ... (WC94=... Wells and Coppersmith, 1994... L14=... Leonard, 2014. (... [31])
 a supprimé:
 a supprimé:
 a supprimé:
 a supprimé:
 a supprimé: average
 a supprimé: 5
 a supprimé:
 1.0 ± 0.4 (
 a supprimé: 2550
 a supprimé: 0.8 ± 0.6
 a supprimé:
 0.6 ± 0.2 / 0.4 ± 0.1
 0.5 ± 0.3 (...and L14) (... [32])
 a supprimé: 2
 a supprimé: ±
 a supprimé: 2550
 a supprimé: 6... ± 0.4 (... [33])
 a supprimé: ±...-0.2 (... [34])
 a supprimé:
 Entire Fault (observed + 10 km) (... [35])
 a supprimé: 5... ± 0.2 / 0.3 (... [37])
 a supprimé: 0.4 ± 0.3
 a supprimé:
 a supprimé: (observed + 5 km) (... [36])
 a supprimé: 6 (WC94)
 a supprimé: 4 ± 0... / 0.3 (... [38])
 a supprimé:
 0.7 ± 0.4
 a supprimé: 0.4 ± 0.2
 a supprimé: ...he timing of the last event,...(between 775 CE and 1778 CE), the inter-event time (between 1610 - 2550 ...nd 3383 yr)... and the slip rate (less than ...ct (... [39])
 a supprimé:

1446 The first results from a local GPS network deployed in the [Ulaanbaatar](#) area since 2010 (Miroshnichenko et al.,
 1447 2018), show a high heterogeneity in direction and velocities, and local complexities. [However, most GPS stations](#)
 1448 [moved \$3 \pm 1\$ mm/ yr. to E-SE, horizontal displacement with respect to Eurasia \(Miroshnichenko et al., 2018\).](#)
 1449 However preliminary, this is consistent with our observations and previous studies that the region absorbs part of
 1450 the deformation along various active faults.

1451 Several slip rates and recurrence times have been estimated and published in western Mongolia (Calais et al. 2003;
 1452 Ritz et al., 2006; Etchebes, 2011; Rizza et al., 2015), focused on faults where large earthquakes (M8+) occurred
 1453 (1905, 1931, 1957) and associated with hundreds of kilometers of surface ruptures (table 5). Their estimated slip
 1454 rate values, [1.5 to 3.8 mm/yr. for geological slip rates and 2 to 2.6 mm/ yr. for geodetic slip rates](#), are about 2 to
 1455 10 times faster than those we estimate on the Sharkhai fault. The recurrence times estimated over there [\(2.43 to 4](#)
 1456 [k yr.\) are of the same order as the inter-time estimated for Sharkhai \(1.6 to 3.4 k yr.\)](#), but the [magnitudes](#) considered
 1457 [in western Mongolia](#) are about 8 and more when it is about 7 for the Sharkhai fault. [The deformation along the](#)
 1458 [Ulaanbaatar region's active faults is much lower than in western Mongolia.](#)

1459 Our results are therefore consistent with other observations in the region. However, our preliminary findings do
 1460 not [favor](#) a specific rupture scenario and associated magnitude for the Sharkhai fault.

1461 [Table 5: Synthesis of geological or geodesic slip rates and recurrence time for large events published for large faults in western](#)
 1462 [Mongolia.](#)

Fault	Geological slip rate (mm/year)	Recurrence time	Geodesic slip rate (mm/year)
Fu-Yun (EQ M8+ in 1931)	3.8 ± 0.2 (Etchebes, 2011)	3 - 4 k yr. (Etchebes, 2011)	2.6 ± 0.5 (Calais et al., 2003)
Bolnay (EQ M8+ in 1905)	3.1 ± 1.7 5 (Rizza et al., 2015)	2.43 - 3.1 k yr. (Rizza, 2010)	2.6 ± 1 (Calais et al., 2003)
Bogd (EQ M8+ in 1957)	1.5 ± 0.26 (Ritz et al., 2006)	3.6 - 3.5 k yr. (Rizza, 2010)	2 ± 1.2 (Calais et al., 2003)

1463

1464 4.3 Implications for Seismic Hazard Model

1465 [Ulaanbaatar is the commercial and industrial center of Mongolia with a concentration of nearly half of the country's](#)
 1466 [total population \(about 3.2 million\), according to the national statistics office of Mongolia, 2018.](#) [The growth of](#)
 1467 [the capital is very important since the last two decades, the population in 1998 being lower than 0.7 million. In](#)
 1468 [terms of seismic risk, the population is spread in buildings with various vulnerability qualities. The masonry](#)
 1469 [structures are major \(62%\) in Ulaanbaatar, steel structures \(18%\), wooden structures and Gers \(2%\). Masonry](#)
 1470 [buildings \(usually apartments\) are considered seismically safe, but the first floor is modified inconsiderately to](#)
 1471 [transform them to shops or restaurants, making the building weaker for seismic resistance \(Dorjpalam et al., 2004\).](#)
 1472 [The stakes and their location are also modified. In the city, new tall buildings have been erected. As the](#)
 1473 [international airport in use since 1957 is too short and too close to the city, a new airport has been constructed 30](#)
 1474 [kilometers to the south of Ulaanbaatar and in operation since mid- 2021.](#)

a supprimé: yr

a supprimé: about twice longer,

a supprimé: magnitude

a supprimé: In western Mongolia, the seismicity (One century of seismicity in Mongolia map, 2000; Dugarmaa and Schlupp, 2000) and slip rates

a supprimé: are higher

a supprimé: the region of Ulaanbaatar.

a supprimé: favour

a supprimé: ¶

a supprimé:

a supprimé: ky

a supprimé: ky

a supprimé: ky

a déplacé (et inséré) [6]

a supprimé: ¶

1489 By this work, we identified and mapped the Sharkhai active fault that has to be included as an earthquake scenario
1490 affecting Ulaanbaatar and its region, and be used in the seismotectonic model for seismic hazard assessment of the
1491 region of Ulaanbaatar and especially in the area of the new airport that will be the place of new constructions. We
1492 suggest considering both scenarios, with the entire fault breaking in one event and the two segments breaking
1493 independently. Our results are the first estimates on this fault for magnitude of large event (6.7 ± 0.2 and 7.1 ± 0.7)
1494 depending on the scenario considered, for their inter-event time (2496 ± 887 yr.) and an attempt for the estimation
1495 of the rate of deformation (between 0.2 ± 0.1 and 0.8 ± 0.6 mm/yr.). If the uncertainties are still substantial, the
1496 estimates are consistent with the regional knowledge.

1497 Our work contributes to the construction of the seismotectonic model, the first step of any seismic hazard
1498 assessment. But the model still faces several unknowns. This fault is a part of a larger system with several parallel
1499 structures, as Hustai and Avdar active faults. The question that arises is if these faults break independently or in a
1500 short time sequence followed by a long period of quiescence. Other active faults in the area have been identified
1501 as Emeel, Gunj, and Ulaanbaatar faults. Are there still other unknown active faults in this area? Are the deformation
1502 rates or inter-event time on all these faults consistent with GPS regional deformation that are, as well, necessary
1503 to be improved with longer measurements? Another challenge is to confirm, by complementary works, all the
1504 estimates recently published, including this work, on some of the active faults in the Ulaanbaatar region. Despite
1505 their uncertainties, all these works already strongly improve the knowledge of active faults in the region, the
1506 seismic hazard assessment and they contribute to the seismic risk mitigation.

1507 For a complete seismic hazard assessment, in addition to the seismotectonic model, propagation and sites effects
1508 (which amplify the ground motion during earthquakes) are also essential especially for Ulaanbaatar located at the
1509 Tuul River Valley on a sedimentary basin of alluvial deposits with a thickness up to 120 m (Odonbaatar 2011,
1510 Tumurbaatar et al., 2019). To answer such questions, future complementary works in the area are still necessary,
1511 which may improve our ability to assess seismic hazard in the region.

1512 **Code/Data availability**

1513 Not applicable.

1514 **Author contribution**

1515 AA and all co-authors contributed to all parts of the work and the manuscript.

1516 **Competing interests**

1517 The authors declare that they have no conflict of interest

1518 **Data and resources**

1520 Pleiades. High resolution (2m Multispectral, 0.5m Panchromatic) were acquired by Pleiades satellites and
1521 broadcast by Astrium.

1522 DEM data: High resolution (12m) topography from DLR's TerraSAR-X / TanDEM-X satellite.

a supprimé: must

a supprimé: now

a supprimé: impacting

a supprimé: . As well, it must

a supprimé: included in

a supprimé: . upgrading the seismotectonic model, associated to an inter-event time of 2080 ± 470 yr for earthquakes with magnitude M_w between 6.4 and 7.1 ± 0.2 , the first estimates on this fault. The

a supprimé: 2

a supprimé: , must be considered.

a supprimé: For that, complementary studies on these active faults are necessary

a déplacé (et inséré) [5]

a supprimé: ¶

1540 Shuttle Radar Topography Mission 1 Arc-Second Global (DOI: /10.5066/F7PR7TFT), last accessed June 2019.

1541 Google Earth views: <http://www.google.com/earth>, last accessed July 2017.

1542 [Radiocarbon dating in in the Poznań Radiocarbon Laboratory- Poland. date of the samples acquisition is 16 July](#)
1543 [2013](#)

1544 [The acquisition dates of satellites images](#)

Figure number	Fig. 7	Fig. A1	Fig. A2	Fig. 9	Fig. A3	Fig. 6	Fig. A4
Image	Pleiades Panchromatic	Google Earth image	Pleiades Panchromatic	Google Earth image	Pleiades Panchromatic	Pleiades MS	Google Earth image
Date of acquisition	October 2012	July 2017	October 2012	June 2020	October 2012	October 2012	June 2014

1545
1546

1547 Acknowledgments

1548 This work was supported in France by the EOST (Ecole et Observatoire des Sciences de la Terre) - IPGS (Institut
1549 de Physique de Globe de Strasbourg, now ITES - Institut Terre et Environnement de Strasbourg), University of
1550 Strasbourg-CNRS and in Mongolia by IAG (Institute of Astronomy and Geophysics, Academy of Sciences of
1551 Mongolia). Access to Pleiades images was supported by CNES (Centre National d'Etudes Spatiales). TanDEM-X
1552 data was kindly provided by DLR (Deutsches Zentrum für Luft- und Raumfahrt) through the TanDEM-X Science
1553 program (Project DEM_OTHER1719). The authors would like to thank the many colleagues and students from
1554 IAG for their help in the field. [We thank Bayarsaikhan Enkhee of IAG for the GPS acquisition used for some 3D](#)
1555 [reconstructions](#). The authors thank Michel Granet for his support of this work, especially during the PhD work of
1556 Abeer Al-Ashkar.

1557

1558 References

1559 [Adiya, M.](#): Seismic activity near Ulaanbaatar: Implication for seismic hazard assessment, Ph.D. thesis, L'Institut
1560 Terre et Environnement de Strasbourg (previously: Institut de Physique du Globe de Strasbourg), France, 256
1561 pages, 29 September 2016.

1562 [Al-Ashkar, A.](#): Tectonique active de la région d'Oulan Bator, Mongolie : Analyse morpho-tectonique et
1563 paléosismologique des failles actives de Sharkhai et Avdar, Ph.D. thesis, L'Institut Terre et Environnement de
1564 Strasbourg (previously : Institut de Physique du Globe de Strasbourg), France, 360 pages, 15 Septembre 2015.

a supprimé: . :

a supprimé: . :

a supprimé:

a supprimé: ¶

- 1568 Bayasgalan, A.: Active tectonics of Mongolia, Ph.D. Thesis, Trinity College Cambridge, 180p, 1999.
- 1569 Bayasgalan A., Jackson J.A., Ritz J.F., and Cartier S.: Field examples of strike-slip fault terminations in Mongolia
1570 and their tectonic significance, *Tectonics*, 18, 394–411, 1999a.
- 1571 Bayasgalan, A. and Jackson, J. A.: A re-assessment of the faulting in the 1967 Mogod earthquakes in Mongolia,
1572 *Geophys. J. Int.*, 138, 784-800, 1999b.
- 1573 Biasi G. P., and Wesnousky S. G.: Steps and gaps in ground ruptures: Empirical bounds on rupture propagation,
1574 *Bull. Seismol. Soc. Am.*, 96, 1110–1124, 2016.
- 1575 Biasi, G. P., and Wesnousky, S. G.: Bends and ends of surface ruptures, *Bulletin of the Seismological Society of*
1576 *America*, 107(6), 2543–2560, <https://doi.org/10.1785/0120160292>, 2017.
- 1577 Calais, E., Vergnolle, M., San'kov, V., Likhnev, A., Miroshnichenko, A., Amarjargal, S., and Déverchère, J.:
1578 GPS measurements of crustal deformation in the Baikal-Mongolia area (1994–2002): Implications for current
1579 kinematics of Asia, *J. Geophys. Res.*, 108, 2501, 2003.
- 1580
1581 [Carpenter N. S. Payne S. J., and Schafer A. L.: Toward reconciling magnitude discrepancies estimated from](#)
1582 [paleoearthquake data, *Seismol. Res. Lett.* 83, 555–565, 2012.](#)
- 1583
- 1584 Crone, A. J. and Haler, K. M.: Segmentation and the co-seismic behavior of Basin and Range normal faults:
1585 examples from east-central Idaho and southwestern Montana U.S.A., *J. Struct. Geol.*, 13, 151–164, 1991.
- 1586
- 1587 Cunningham, W.D.: Cenozoic normal faulting and regional doming in the southern Hangay region, Central
1588 Mongolia: implications for the origin of the Baikal rift province, *Tectonophysics*, 331, pp. 389-411, 2001.
- 1589
- 1590 Cunningham, W.D.: Structural and topographic characteristics of restraining-bend mountain ranges of Altai, Gobi
1591 Altai and easternmost Tien Shan. In: Cunningham W.D., & Mann P. (Eds.), *Tectonics of strike-slip restraining*
1592 *and releasing bends*, *Geol. Soc., London, Special Publications*, pp. 219–237, 2007.
- 1593 Cunningham, W.D., Windley, B.F., Dorjnamjaa, D., Badamgarov, G., and Saandar, M.: A structural transect across
1594 the Mongolian Altai: Active transpressional mountain building in central Asia, *Tectonics*, 15, 142-156, 1996.
- 1595 [Demberel, S., Batarsuren, G., Imaev, V.S. et al.: Paleoseismology deformations around ulan bator according to](#)
1596 [geological and geophysical data. *Seism. Instr.* 47, 314–320. <https://doi.org/10.3103/S0747923911040025>, 2011.](#)
- 1597 De Polo, C. M., Clark, D.G., Slemmons, D.B. and Rameli, A. R.: Historical surface faulting in the Basin and Range
1598 province, western North America-implication for fault segmentation, *Journal of Structural Geology*, 13, 1991.
- 1599 Dorjpalam, S., Kawase, H., Ho, N.: Earthquake Disaster Simulation for Ulaanbaatar, Mongolia Based on The Field
1600 Survey and Numerical Modeling of Masonry Buildings, 13th World Conference on Earthquake Engineering
1601 Vancouver, B.C., Canada, [paper No. 461](#), 2004.

- 1603 Dugarmaa, T. and Schlupp, A.: One century of seismicity in Mongolia map (1900–2000), in: Proc. MAS 4, No.
1604 170, pp. 7–14, 2000.
- 1605 Dujardin, J.R, Bano, M., Schlupp, A., Ferry, M., Ulziibat, M., Tsend-Ayush, N., and Enkhee B.: GPR
1606 measurements to assess the Emeelt active fault's characteristics in a highly smooth topographic context, Mongolia,
1607 Geophys. J. Int, <https://doi.org/10.1093/gji/ggu130>, 2014.
- 1608 Etchebes, M. : Paléosismologie spatiale : segmentation et scénarios de ruptures sismiques La faille de Fuyun et la
1609 faille du Kunlun, Chine, Ph.D. thesis, Institut de Physique du Globe de Paris (IPGP), France, 400pp, 2011.
- 1610 Finzi, Y. and Langer, S.: Damage in stop-overs may enable large cascading earthquakes, Geophysical Research
1611 Letters, 39: L16303. DOI: 10.1029/2012GL052436, 2012.
- 1612 Feng, Z. D., Zhai, X. W., Ma, Y. Z., Huang, C. Q., Wang, W. G., Zhang, H. C. et al. : Eolian environmental
1613 changes in the Northern Mongolian Plateau during the past ~ 35,000 yr., *Palaeogeography, Palaeoclimatology,*
1614 *Palaeoecology* 245(3-4): 505-517, 2007.
- 1615 Ferry, M., Schlupp, A., Munkhuur, U., Munschy, M., Fleury, S., Baatarsuren G., Erdenezula, D., Munkhsaikhan,
1616 A., and Ankhtsetseg, D.: Tectonic Morphology of the Hustai Fault (Northern Mongolia), A Source of Seismic
1617 Hazard for the city of Ulaanbaatar, EGU General Assembly, Vienna, Austria, 2010.
- 1618 Ferry, M., Schlupp, A., Munkhuur, U., Munschy, M., and Fleury, S.: Tectonic morphology of the Hustai Fault
1619 (Northern Mongolia), EGU General Assembly, Vienna, Austria, 2012.
- 1620 Fleury, S., Munschy, M., Schlupp, A., Ferry, M., Bano, M., and Munkhuu, U.: High-resolution magnetic survey
1621 to study Hustai Fault (northern Mongolia), AGU Fall Meeting, San Francisco, California, USA, 2011.
- 1622 Fleury, S., Munschy, M., Schlupp, A., Ferry, M., and Munkhuu, U.: High resolution magnetic survey across the
1623 Emeelt and Hustai faults near Ulaanbaatar, Mongolia, EGU General Assembly, Vienna, Austria, 2012.
- 1624 Harris, R. A., Archuleta, R. J. and Day, M.: Fault steps and the dynamic rupture process: 2-D digital simulations
1625 of a spontaneously propagating shear fracture, *Geophys. J. Int.*, 18, 893–896, 1991.
- 1626 Imaev, V.S., Smekalin, O.P., Strom, A.L., Chipizubov, A.V., and Syas'ko, A.A.: Seismic-hazard assessment for
1627 Ulaanbaatar (Mongolia) on the basis of seismogeological studies, *Russian Geology and Geophysics*, 53, 9, 906-
1628 915, 2012.
- 1629 Khilko, S.D., Kurushin, R.A., Kochetkov, V.M., Misharina, L.A., Melnikova, V.I., Gilyova, N.A., Lastochkin,
1630 S.V., Baljinnyam, I., and Monhoo D.: Earthquakes and the base of the seismic zoning of Mongolia, The joint
1631 Soviet-Mongolian scientific - Research Geological Expedition, 41, 225 pages, 1985.
- 1632 Klinger Y.: Relation between continental strike-slip earthquake segmentation and thickness of the crust, *J.*
1633 *Geophys. Res.*, 115: B07306. DOI: 10.1029/2009jb006550, 2010.

a supprimé: |

a supprimé: |

- 1635 Leonard, M.: Self-consistent earthquake fault scaling relations: Update and extension to stable continental strike
1636 slip faults, *Bull. Seismol. Soc. Am.*, 104(6), 2953–2965, 2014.
- 1637 Lettis, W., Bachhuber, J., Witter, R., Brankman, C., Randolph, C. E., Barka, A., Page, W. D., and Kaya, A.:
1638 Influence of Releasing Step-Overs on Surface Fault Rupture and Fault Segmentation: Examples from the 17
1639 August 1999 Izmit earthquake on the North Anatolian Fault, Turkey, *Bull. Seismol. Soc. Am.*, 92, 19–42, 2002.
- 1640 [Majer Z. and Teleki K.: Monasteries and Temples of Bogdiin Kh̄ree, Ikh Kh̄ree or Urga, the Old Capital City
1641 of Mongolian in the First Part of the Twentieth Century, Ulaanbaatar, 2006](#)
- 1642 Manandhar, S., Hino, T., and Kitag, K.: Influences of Long-Term Tectonic and Geo-Climatic Effects on
1643 Geotechnical Problems of Soft Ground - Ulaanbaatar, Mongolia, *Lowland Technology International*, 18(1): 51-58
1644 *International Association of Lowland Technology (IALT): ISSN 1344-9656, 2016.*
- 1645 Miroshnichenko, A.I., Radziminovich, N.A., Lukhnev, A.V., Zuev, F.L., Demberel, S., Erdenezul, D., and
1646 Ulziibat, M.: First results of GPS measurements on the Ulaanbaatar geodynamic testing area, *Russian Geology
1647 and Geophysics* 59, 1049–1059, 2018.
- 1648 Nuramkhaan, B., Nakane, Y., Yamasaki, S., Otgonbaatar, J., Nuramkhaan, M., Takeuchi, M., Tsukada, K.,
1649 Katsurada, Y., Gonchigdorj, S., and Sodnom, K.: Description of a NW trending brittle shear zone, Ulaanbaatar,
1650 Mongolia. *Bull. Nagoya Univ. Museum*, No. 28, 39–43, 2012.
- 1651 One century of seismicity in Mongolia map (1900 - 2000): Coordinators: Dr. Dugarmaa, T., and Dr. Schlupp, A.
1652 ; Authors: Adiya M., Ankhtsetseg D., Baasanbat Ts., Bayar, G., Bayarsaikhan, Ch., Erdenezul, D., M̄nḡöns̄üren,
1653 D., M̄nkh̄saikhan, A., M̄nkh̄ö, D., Narantsetseg, R., Odonbaatar, Ch., Selenge, L., Dr. Tsembe, B., Ölz̄ibat,
1654 M., Urtnasan, Kh. and in collaboration with DASE and (RCAG)
- 1655 Odonbaatar Chimed: Site effects characterization in the basin of Ulaanbaatar, Ph.D. thesis, Université de
1656 Strasbourg- France, 184p., <https://tel.archives-ouvertes.fr/tel-00785708>, 2011.
- 1657 Parfeevets, A.V. and Sankov, V.A. : Late Cenozoic tectonic stress fields of the Mongolian microplate Champs de
1658 contraintes tectoniques fini-cénozoïques dans la microplaque de Mongolie, *Comptes Rendus Géoscience*, Volume
1659 344, Issues 3–4, Pages 227-238, 2012.
- 1660 Poliakov, A. N. B., Dmowska, R., and Rice, J. R.: Dynamic shear rupture interactions with fault bends and off-
1661 axis secondary faulting, *J. Geophys. Res.* 107(B11), 2295, doi: [10.1029/2001JB000572](https://doi.org/10.1029/2001JB000572), 2002.
- 1662 Ramsey, B.C. and Lee, S.: Recent and Planned Developments of the Program OxCal. *Radiocarbon*, Volume 55,
1663 Issue 2: Proceedings of the 21st International Radiocarbon Conference (Part 1 of 2), pp.720–730, DOI:
1664 <https://doi.org/10.1017/S0033822200057878>, 2013.
- 1665 Reimer, P. et al.: IntCal13 and Marine13 Radiocarbon Age Calibration Curves 0–50,000 Years calBP,
1666 *Radiocarbon*, 55, 1869–1887, 2013.

a supprimé:

a supprimé:

a supprimé:

- 1669 Ritz, J.-F., Bourle 's, D., Brown, E.T., Carretier, S., Chery, J., Enhtuvshin, B., Galsan, P., Finkel, R.C., Hanks,
 1670 T.C., Kendrick, K.J., Philip, H., Raisbeck, G., Schlupp, A., Schwartz, D.P., Yiou, F.: Late Pleistocene to Holocene
 1671 slip rates for the Gurvan Bulag thrust fault (Gobi-Altay, Mongolia) estimated with 10Be dates, *J. Geophys. Res.*,
 1672 108 (B3), p. 2162, 2003.
- 1673 Ritz, J. F., Braucher, R., Brouw, E. T., Carretier, S., and Bourlès, D. L.: Using in situ-produced 10Be to quantify
 1674 active tectonics in the Gurvan Bogd mountain range (Gobi-Altay, Mongolia), *Geological.*, 415, 87–110, 2006.
- 1675 Rizza, M.: *Analyses des vitesses et des déplacements co-sismiques sur des failles décrochantes en Mongolie et en*
 1676 *Iran*, Ph.D. thesis, université Montpellier II, France, 408 pages, 5 décembre 2010.
- 1677 Rizza, M., Ritz, J.-F., Braucher, R., Vassallo, R., Prentice, C., Mahan, S., McGill, S., Chauvet, A., Marco, S.,
 1678 Todbileg, M., Demberel, S., Bourlès D.: Slip rate and slip magnitudes of past earthquakes along the Bogd left-
 1679 lateral strike-slip fault (Mongolia), *Geophys. J. Int.*, 186, 897–927, 2011.
- 1680 Rizza, M., Ritz, J.-F., Prentice, C., Vassallo, R., Braucher, R., Larroque, C., Arzhannikova, A., Arzhannikov, S.,
 1681 Mahan, S., Massault, M., Michelot, J.-L., Todbileg, M., and ASTER Team: Earthquake Geology of the Bulnay
 1682 Fault (Mongolia). *Bull. Geol. Soc. Am.*, 105, 2015.
- 1683 Schlupp, A. : *Néotectonique de la Mongolie Occidentale analysée à partir de données de terrain, sismologiques et*
 1684 *satellites*, Ph.D. Thesis, Louis Pasteur university, Strasbourg, France, 256pp, 1996.
- 1685 Schlupp, A., Ferry M., Munkhuu, U., Munsch, M., Fleury, S., Adiya, M., Bano, M., and Baatarsuren, G.: The
 1686 Emeelt active fault, revealed by the outbreak of micro seismicity, and its impact on the PSHA of Ulaanbaatar,
 1687 capital of Mongolia, Part I: seismotectonic analysis, ESC General Assembly, Montpellier, France, 2010a.
- 1688 Schlupp, A., Ferry, M., Munkhuu, U., Munsch, M., and Fleury, S.: Tectonic Morphology of the Hustai Fault
 1689 (Northern Mongolia): Implications for Regional Geodynamics, AGU Fall Meeting, San Francisco, USA, 2010b.
- 1690 Schlupp, A., Ferry, M., Ulziibat, M., Baatarsuren, G., Munkhsaikhan, A., Bano, M., Dujardin, J.-M., Nyambayar,
 1691 Ts., Sarantsetseg, L., Munsch, M., Fleury, S., Mungunshagai, M., Tserendug, Sh., Nasan-Ochi, T., Erdenezul,
 1692 D., Bayarsaikhan, E., batsaikhan, Ts., and Demberel, S.: Investigation of active faults near Ulaanbaatar,
 1693 Implication for seismic hazard assessment, ASC General Assembly of Asian Seismological Commission,
 1694 Ulaanbaatar, Mongolia, 2012.
- 1695 [Suzuki, Y., T. Nakata, M. Watanabe, S. Battulga, D. Enkhtaivan, S. Demberel, C. Odonbaatar, A. Bayasgalan, and](#)
 1696 [T. Badral. Discovery of Ulaanbaatar Fault: A New Earthquake Threat to the Capital of Mongolia, *Seismol. Res.*](#)
 1697 [Lett.XX, 1–11, doi: 10.1785/0220200109, 2020](#)
- 1698 Takeuchi, M., Tsukada, K., Suzuki, T., Nakane, Y., Sersmaa, G., Manchuk, N., Kondo, T., Matsuzawa, N., Bacht,
 1699 N., Khishigsuren, S., Onon, G., Katsurada, Y., Hashimoto, M., Yamasaki, S., Matsumoto, A., Oyu-Erdene, B.,
 1700 Bulgantsetseg, M., Kundyz, S., Enkhchimeg, L., Ganzorig, R., Myagmarsuren, G., Jamiyandagva, O., and

a supprimé: . :

a supprimé:

a supprimé: ¶

1703 Molomjamts, M.: Stratigraphy and geological structure of the Palaeozoic system around Ulaanbaatar, Mongolia,
1704 Bulletin of the Nagoya University Museum, No.28, 1-18, 2013.

a supprimé:

1705 Tomurtogoo, O., Byamba, J., Badarch, G., Minjin, Ch., Orolmaa, D., Khosbayar, P., and Chuluun, D.: Geologic
1706 map of Mongolia. Scale 1:1000000. Mineral Resources Authority of Mongolia, Ulaanbaatar, 1998.

1707 Tumurbaatar, Z., Miura, H., Tsamba, T.: Site Effect Assessment in Ulaanbaatar, Mongolia through Inversion
1708 Analysis of Microtremor H/V Spectral Ratios, Geosciences, 9, 228; doi: 10.3390/geosciences, 9050228, 2019.

1709 Walker, R.T., Molor, E., Fox, M., Bayasgalan, A.: Active tectonics of an apparently aseismic region: distributed
1710 active strike-slip faulting in the Hangay Mountains of central Mongolia, Geophys. J. Int., 174, pp. 1121-1137,
1711 2008.

1712 Wells, D. L. and Coppersmith, K. J.: New Empirical Relationships among Magnitude, Rupture Length, Rupture
1713 Width, Rupture Area, and Surface Displacement, Bull. Seismol. Soc. Am., 84, 974-1002, 1994.

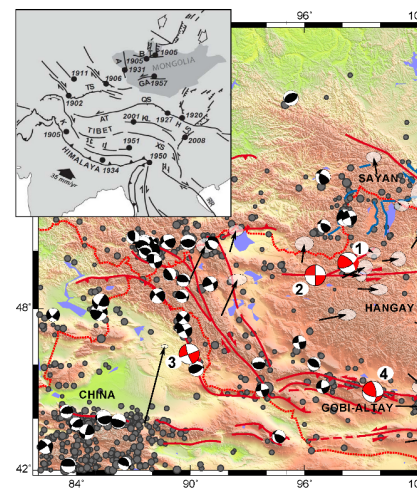
1714 Wesnousky Steven G.: Predicting the endpoints of earthquake ruptures, Nature, 444, 358-360. DOI:
1715 10.1038/nature05275, 2006.

a supprimé:

1716 [Wesnousky S. G.: Displacement and geometrical characteristics of earthquake surface ruptures: Issues and
1717 implications for seismic-hazard analysis and the process of earthquake rupture, Bulletin of the Seismological
1718 Society of America, 98 \(4\), 1,600-1,632, 2008.](#)

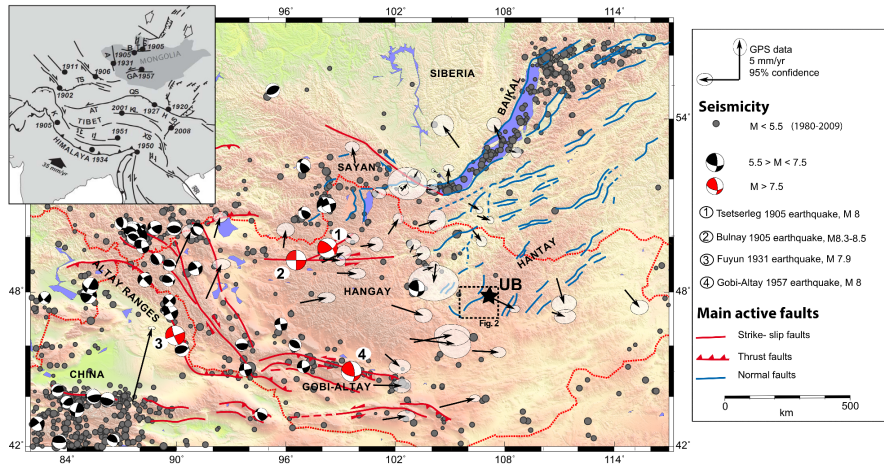
a supprimé:

1719



a supprimé:

1726
1727

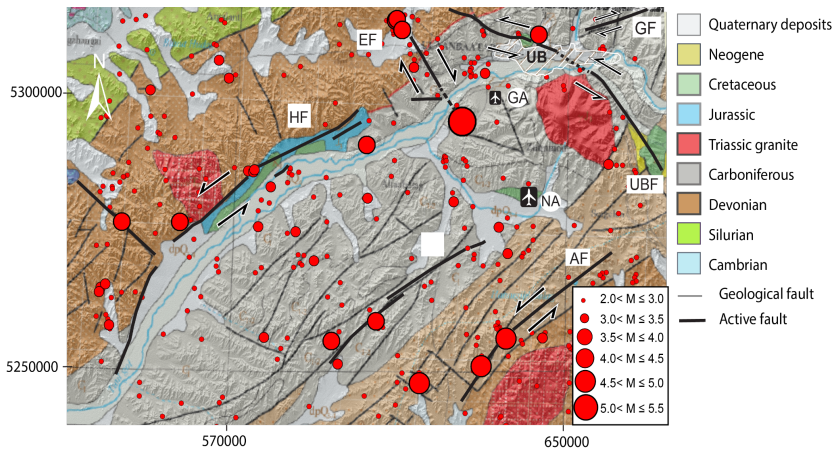


1728
1729
1730
1731
1732
1733
1734

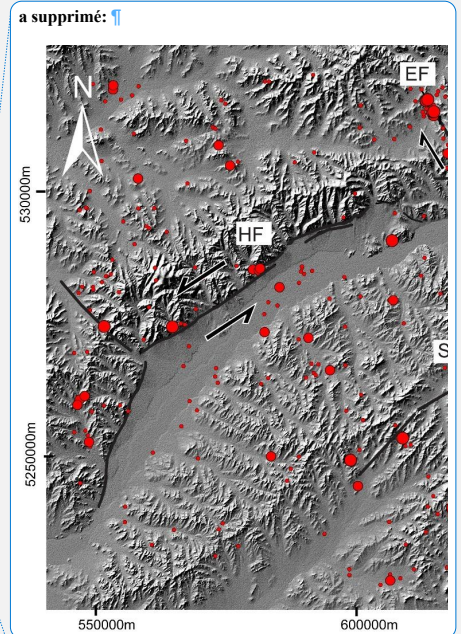
Figure 1: Tectonic map of Mongolia (modified from Rizza et al., 2015). The four great earthquakes of magnitude 8+ that occurred since 1905 are labeled 1 to 4. The inset map shows active deformations in Asia with Mongolia between the India-Asia collision to the south and extensive structures of the Baikal Rift to the north. "UB" is Ulaanbaatar, capital of Mongolia and the rectangle shows the location of Fig. 2.

- a supprimé: showing the major active faults and seismic activity with centroid moment tensor solutions (adapted from
- a supprimé: Gray dots are the epicenter of earthquakes that happened between 1980 and 2008. Not the
- a supprimé: (labeled 1 to 4)
- a supprimé: .
- a supprimé: . Note the position of
- a supprimé: at
- a supprimé: at
- a supprimé: The black circle shows the major earthquakes (M ≥ 8). The
- a supprimé: area in

a supprimé: |

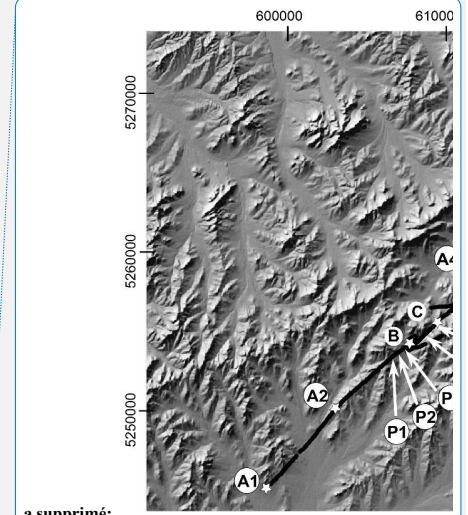
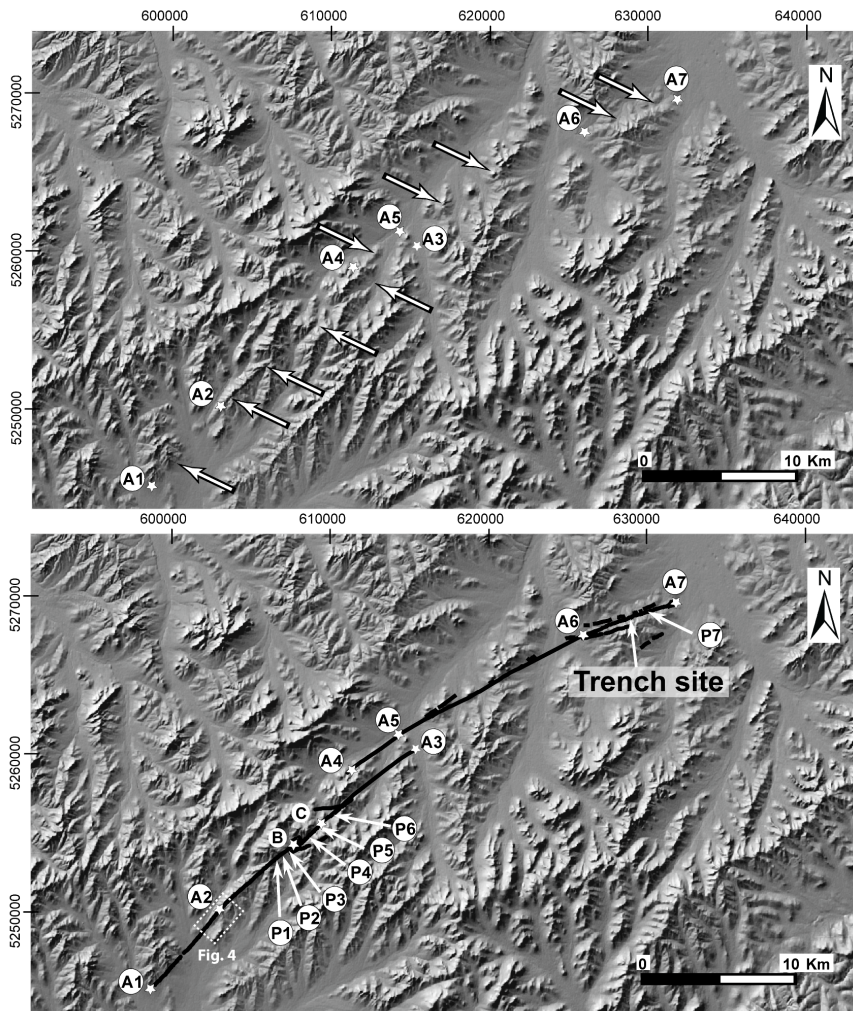


1747
 1748 **Figure 2:** Geological and seismo-tectonic context of the Ulaanbaatar region. Red dots are earthquakes recorded between 1994
 1749 and 2011 (Institute of Astronomy and Geophysics, Mongolian Academy of Sciences, National Data Center). Black lines
 1750 represent the active faults (HF: Hustai fault, EF: Emeelt fault, SF: Sharkhai fault, AF: Avdar fault, UBF: Ulaanbaatar fault,
 1751 GF: Gunj fault). UB: Ulaanbaatar city, GA: Ghingis Khan old international airport, NA: new international airport. The
 1752 background DEM is from SRTM1 data (see data and resources). Geological map is an extract from Geologic map of Mongolia
 1753 (scale 1:1 M) (Tomurtogoo et al, 1998).



- a supprimé: [1]
- a supprimé: Seismic activity observed in
- a supprimé: area of
- a supprimé: from the IAG-MAS NDC
- a supprimé: The black
- a supprimé: .
- a supprimé: =
- a supprimé: Seismic swarms are concentrated along the Emeelt fault. ...
- a supprimé: [1]
- ... [40]
- a supprimé: of the area of Ulaanbaatar and surroundings modified from ...
- a supprimé: . Scale
- a supprimé: .000000
- a supprimé: GF: Gunj fault, EF: Emeelt fault, HF: Hustai fault and SF: Sharkhai fault AF: Avdar fault. The AF, SF, and HF are in a large post carboniferous synclinal. Note th... [41]

a supprimé: [1]

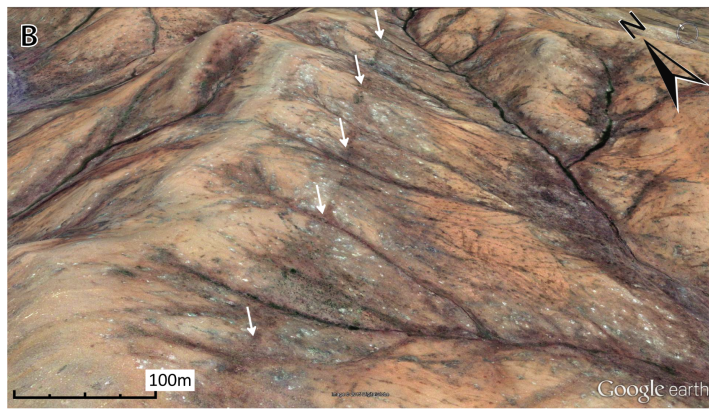
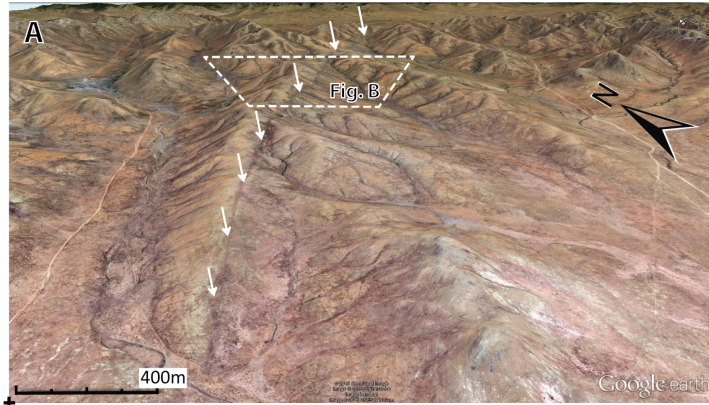


a supprimé:
Figure 4: The

1783
1784
1785
1786
1787
1788

Figure 3: Top: SRTM1 DEM (see data and resources) with arrows showing the location of the Sharkhai active fault. Bottom: Simplified map of the Sharkhai active fault about 46 km long and strikes from N42° at south to N72° at north. Letters A1-A7, B and C indicate the location of sites described in the text. Letters P1 to P7 indicate the locations of documented offset drainages. Note the left step-over which divides the fault in two sections between points A3 and A4. Coordinates are in UTM zone 48N.

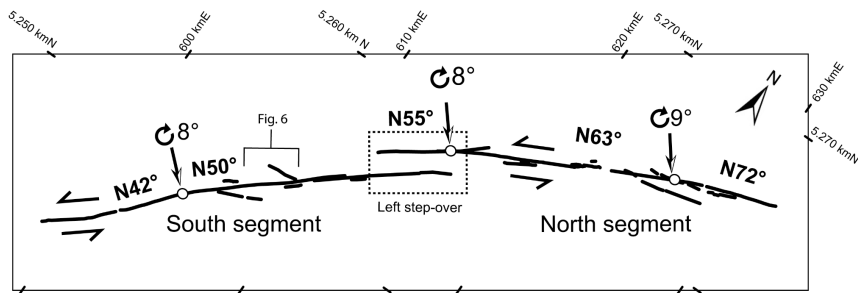
- a supprimé: identified at surface is
- a supprimé: between 42° and 72° NE.
- a supprimé: (
- a supprimé:) and stars
- a supprimé: coordinate points
- a supprimé: P1, P2, P3, P4, P5, P6 and
- a supprimé: are shifted drainages
- a supprimé: .
- a supprimé: , south
- a supprimé: north sections. The background DEM is from SRTM1 data, coordinates
- a supprimé: (see data and resources).
- a supprimé: [



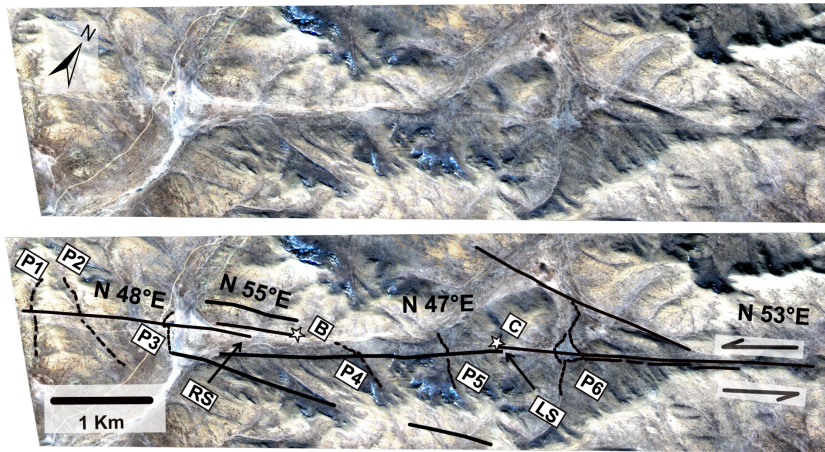
1803
 1804 **Figure 4:** 3D images showing the geomorphology of the Sharkhai fault (white arrows) at its southern end (see Fig. 3 for
 1805 location). The fault is well identified at regional scale (top image) but the fault trace is smoothed by erosion and shows no clear
 1806 scarp locally (images from Google Earth).

1807
 1808

a supprimé: |



1809 **Figure 5:** Map of the fault trace and major strike changes (according to the average direction of every segment). Dashed
 1810 rectangle is the left step-over which divides the fault in two main segments, southern and northern segments with a local 5°
 1811 clockwise strike change (from 50° N to 55° N). The average strike change between the southern and northern segments is
 1812 larger, with 13° clockwise (50° N to 63° N). Secondary branches parallel or oblique to the fault with direction varying between
 1813 56° and 83°. Coordinates are in UTM zone 48N.



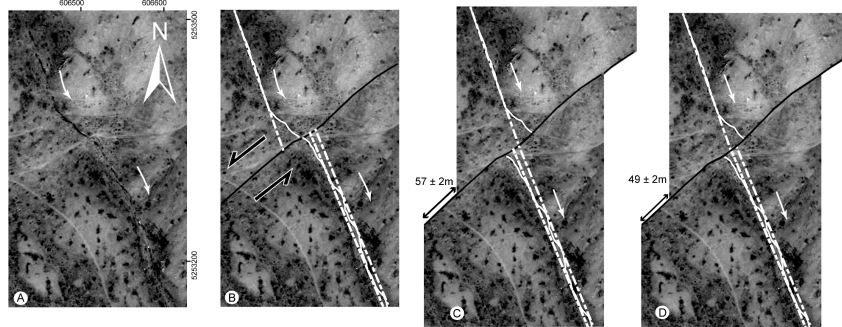
1816 **Figure 6:** Fault map (black lines) covering the central part of the southern section. P1, P2, P3, P4, P5 and P6 are offset
 1817 drainages. Left step-over (LS) and right step-over (RS) are of 173 m and 61 m width respectively. The strike changes locally
 1818 from N47° to N55°. Several secondary branches of lengths between 190 m and 1.6 km are either parallel or oblique to the main
 1819 rupture. Background is a 2-m-resolution RGB Pleiades satellite image. See text for details and Fig. 5 for location.

a déplacé (et inséré) [11]

a déplacé (et inséré) [12]

a supprimé: [1]

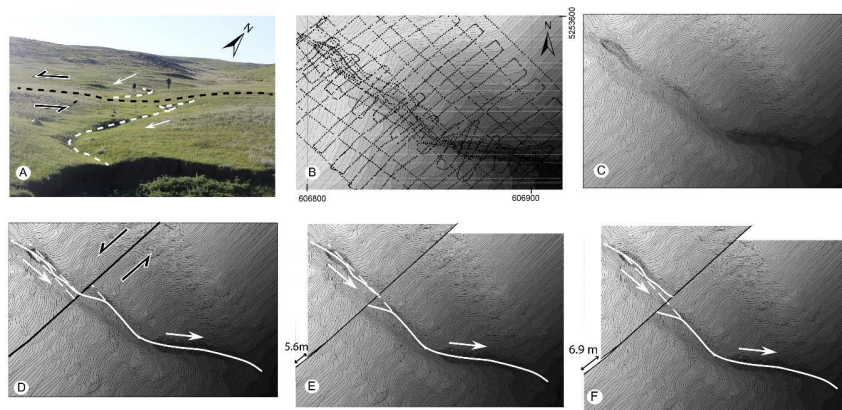
1823



1824

1825 **Figure 7:** Offset reconstruction for drainage P1. A) Present-day situation: Panchromatic Pleiades image displaying the shifted drainage. B) Present-day situation with drainage and fault. C) and D) Reconstruction of the drainage to its initial position after back-slip along the fault. The maximum cumulative offset measured is 57 ± 2 m (C) and the minimum is 49 ± 2 m (D). Hence the left-lateral offset is estimated at 53 ± 6 m. The uncertainty combines measurement errors (2 m) and data resolution uncertainty (1 m). For location, see Fig. 3.

1830

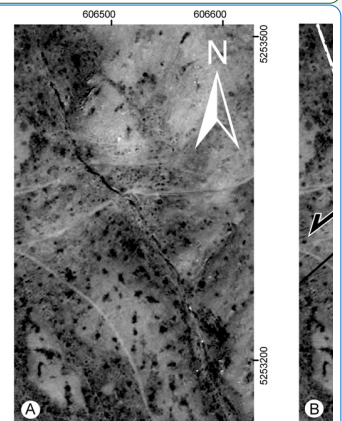


1831

1832 **Figure 8:** Offset reconstruction for drainage P2. A) Field photograph of P2: the black dashed line indicates the fault trace. The north direction in the photograph is approximate. B) Differential GPS measurements used to build the digital topographic map. C) Digital topographic map based on GPS measurements. D) Present-day situation: the offset is measured on images by projecting the average upstream and the downstream to the fault trace. We consider for the upstream a "wide zone" giving an uncertainty on its piercing position for the back-slip reconstruction. E) Minimum back-slip reconstruction of 5.6 m. F) Maximum back-slip reconstruction of 6.9 m. Hence, the left-lateral offset is estimated at 6.25 ± 1.65 m. White arrows: water flow direction. For location, see Fig. 3.

1839

a déplacé (et inséré) [13]



a supprimé:

[... [42]

a déplacé vers le haut [13]: A) Present-day situation: Panchromatic Pleiades image displaying the shifted drainage.

a supprimé: : the offset is measured on images by projecting the average upstream and the downstream to the fault trace. C... C) and D) Reconstruction of the drainage to its initial position after back-slip along the fault. The uncertainty of... maximum cumulative offset measured is 57 ± 2 m (... [43]

a supprimé:

a déplacé (et inséré) [14]

a supprimé: 6...: Offset of... reconstruction for drainage P2. A) Photograph (... [44]

a déplacé vers le haut [14]: The north direction in the photograph is approximate. B) Differential GPS measurements used to build the digital topographic map.

a supprimé: If we consider the minimum... minimum back-slip, we measure... reconstruction of 5.6 m and... F) if we consider the maximum... maximum back slip, we measure... reconstruction of 6.9 m. Hence... the left-lateral offset is estimated at 6.25 ± 1.65 m. White arrows: water flow direction. For location, see Fig. 3. (... [45]

a supprimé:Saut de page.....

[... [46]

a supprimé:

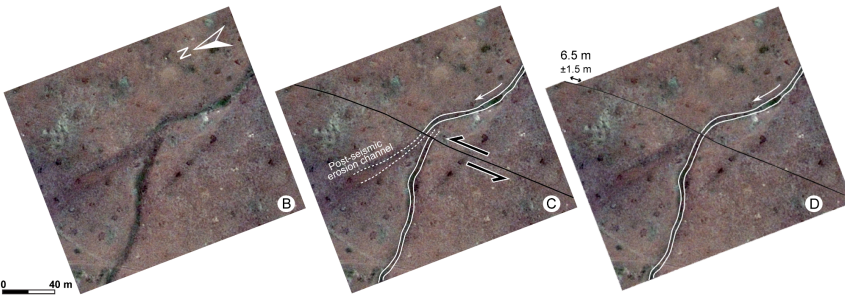
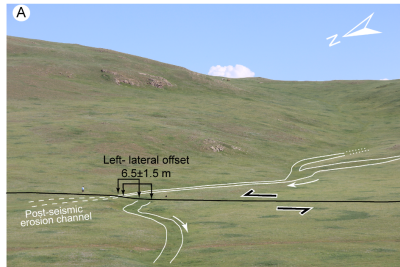
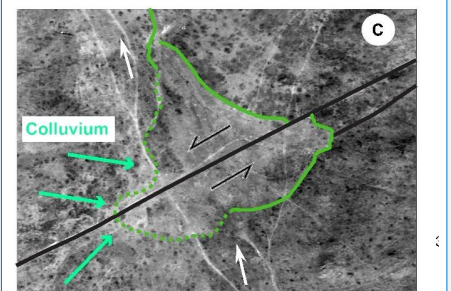
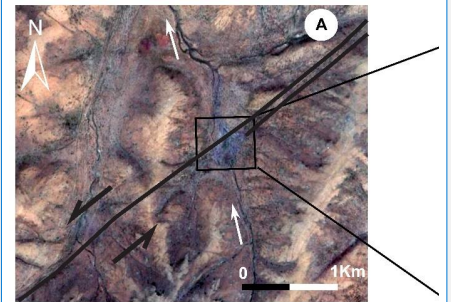


Figure 9: Offset reconstruction for drainage P5. A) Field photograph: the black line indicates the fault trace and the white lines mark the edges of the P5 channel. The north direction in the photograph is approximate. B) Panchromatic Pleiades image of P5. C) Present-day situation with the fault (black line) and the paleo river (white lines) disconnected across the fault. Note the post-seismic erosion due to the upstream flow that crosses the fault. D) Reconstruction of the drainage to its initial situation yields 6.5 ± 1.5 m of cumulative left-lateral offset. The uncertainty combines measurement errors (2 m) and data resolution uncertainty (1 m). For location see Fig. 3.

- a supprimé: of
- a supprimé: on the Sharkhai fault. A) Photograph of shifted drainage:
- a supprimé: .
- a supprimé: overlapped
- a supprimé: when crossing
- a supprimé: 0
- a supprimé: associated with the offset estimation is obtained by realizing several retro-deformations.
- a supprimé: 4



- a supprimé: 1

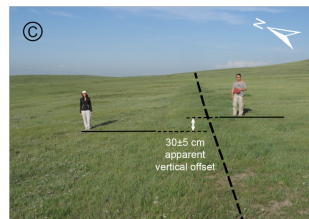
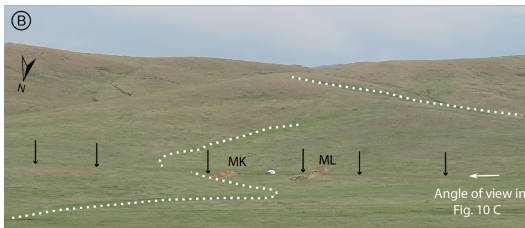
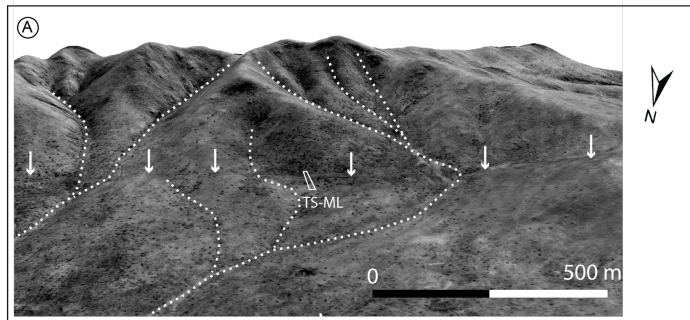


Figure 10: A) 3D perspective view from panchromatic Pleiades image (0.5 m resolution) draped TanDemX DEM (12 m resolution) shows the Muka-L trench site (TS-ML), the fault trace (white arrows) and the temporary drainages (dashed white lines). B) Field photograph of the trench site (ML=Muka-L and MK=Muka-K excavations). C) Field photograph looking east along the fault, before excavation, shows the fault trace (dashed line) marked by well-developed vegetation. Note the small component of apparent vertical movement (30 ± 5 cm). For location see Fig. 3.

a supprimé: Left-lateral offset affecting Quaternary deposits (P6 at 609957.1 m E , 5256060.72 m N).

a déplacé vers le haut [11]: Left step-over (LS) and right step-over (RS) are of 173 m and 61 m width respectively. The strike changes locally from N47° to N55°. Several secondary branches of lengths between 190 m and 1.6 km are either parallel or oblique to the main rupture.

a supprimé: Google earth imagery (see data and sources) overlapped with the surface rupture and the location of the images B to D. B) Panchromatic image. C) Present-day situation. Panchromatic image overlapped with the fault traces marked with black lines and Quaternary deposits trapped (green limits). The SW side of the trapped Quaternary deposits has been covered by lateral colluions

a supprimé: NW hill (light green arrows) hiding the real limit of Quaternary trapped deposits (dashed green line). D) Reconstruction of the NE side of the Quaternary trapped deposit to its initial situation shows a 36 ± 1 m of cumulative left lateral offset (White arrows indicate drainage direction). For location see Fig. 4.

... [47]

a supprimé: In background,

a supprimé: satellites images (multispectral RGB-NIR) with 2

a supprimé: .

a déplacé vers le haut [12]: See text for details and Fig.

a supprimé: 4 for location.

... [48]

a supprimé: DEM (TanDemX data at 12 m resolution, see Data and Resources

a supprimé: Location

a supprimé:) on the north segment of the Sharkhai fault.

a supprimé: taken from the west to the

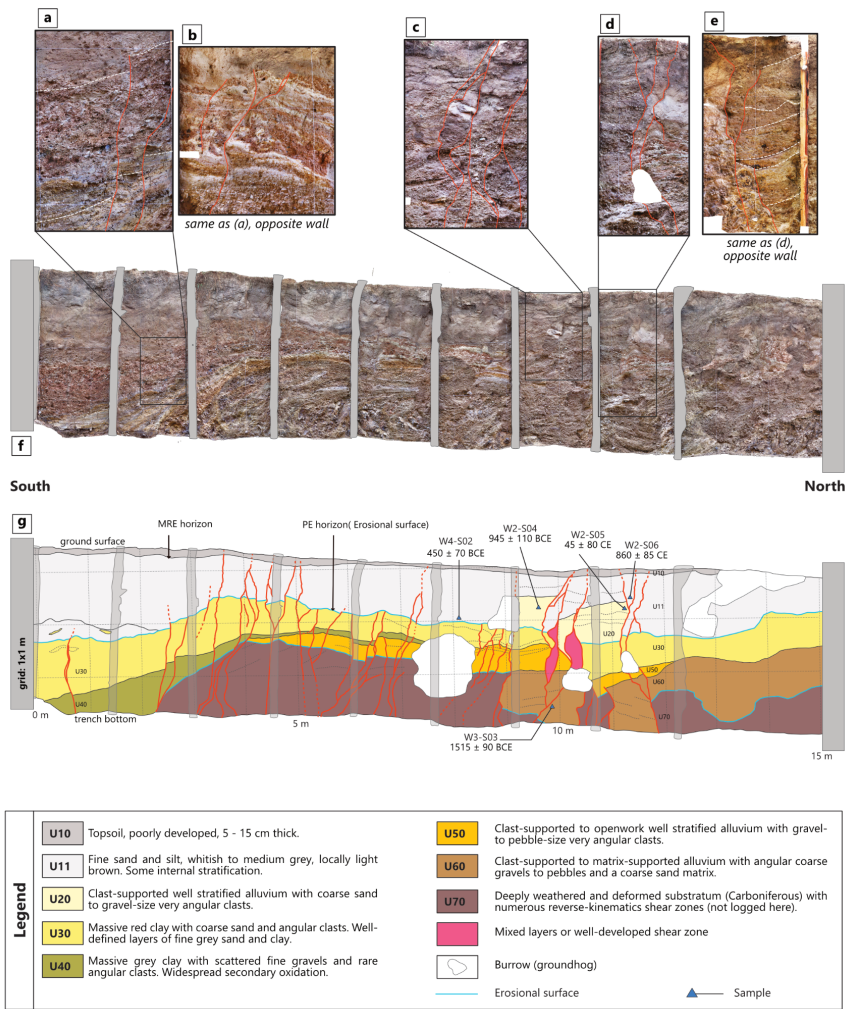
a supprimé: a

a supprimé: contrast (Dashed line). We can note the

a supprimé: about

a supprimé: 4

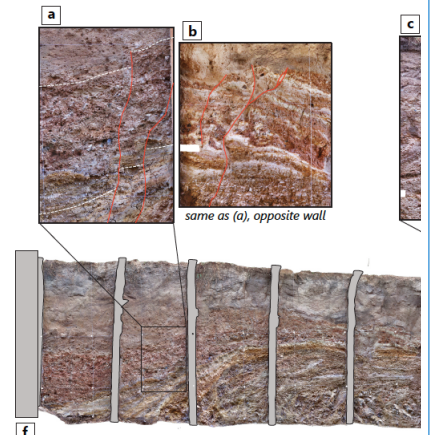
a supprimé: ¶



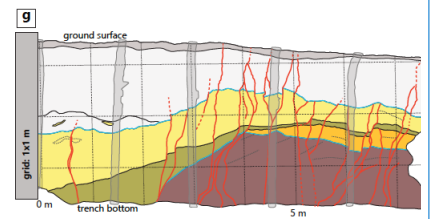
2075
2076
2077
2078
2079
2080

Figure 11: Muka-L trench exposure. a) to e): Close-ups showing deformation features (step-like geometry, geometry resembling flower structures, apparent offsets). f) General orthophoto mosaic of the west wall, originally rendered at 1 mm resolution. g) Detailed paleoseismic log of the west wall. The ruptures associated with the last two events are in red. Event horizons are shown for the most recent event (MRE) and the penultimate event (PE). See text for details.

a supprimé:



South



Legend	
U10	Topsoil, poorly developed, 5 - 15 cm thick.
U11	Fine sand and silt, whitish to medium grey, locally light brown. Some internal stratification.
U20	Clast-supported well stratified alluvium with coarse sand to gravel-size very angular clasts.
U30	Massive red clay with coarse sand and angular clasts. Well-defined layers of fine grey sand and clay.
U40	Massive grey clay with scattered fine gravels and rare angular clasts. Widespread secondary oxidation.

a supprimé: 15:

a supprimé: orthophotomosaic

a supprimé:

Page 2 : [1] a supprimé Authors 05/01/2022 15:57:00



Page 2 : [1] a supprimé Authors 05/01/2022 15:57:00



Page 2 : [1] a supprimé Authors 05/01/2022 15:57:00



Page 2 : [1] a supprimé Authors 05/01/2022 15:57:00



Page 2 : [1] a supprimé Authors 05/01/2022 15:57:00



Page 2 : [2] Déplacé depuis la page 2 (Déplacement n°2) Authors 05/01/2022 15:57:00

[based on geodetic data \(Calais et al., 2003\).](#)

Page 2 : [2] Déplacé depuis la page 2 (Déplacement n°2) Authors 05/01/2022 15:57:00

[based on geodetic data \(Calais et al., 2003\).](#)

Page 2 : [3] a supprimé Authors 05/01/2022 15:57:00



Page 2 : [3] a supprimé Authors 05/01/2022 15:57:00



Page 2 : [3] a supprimé Authors 05/01/2022 15:57:00



Page 2 : [4] a supprimé Authors 05/01/2022 15:57:00



Page 2 : [4] a supprimé Authors 05/01/2022 15:57:00



Page 2 : [5] a supprimé Authors 05/01/2022 15:57:00



Page 2 : [5] a supprimé Authors 05/01/2022 15:57:00



Page 2 : [5] a supprimé Authors 05/01/2022 15:57:00



Page 2 : [5] a supprimé Authors 05/01/2022 15:57:00



Page 2 : [5] a supprimé Authors 05/01/2022 15:57:00



Page 2 : [5] a supprimé Authors 05/01/2022 15:57:00



Page 2 : [5] a supprimé Authors 05/01/2022 15:57:00



Page 2 : [5] a supprimé Authors 05/01/2022 15:57:00



Page 2 : [5] a supprimé Authors 05/01/2022 15:57:00



Page 2 : [5] a supprimé Authors 05/01/2022 15:57:00



Page 2 : [5] a supprimé Authors 05/01/2022 15:57:00



Page 2 : [5] a supprimé Authors 05/01/2022 15:57:00



Page 2 : [5] a supprimé Authors 05/01/2022 15:57:00



Page 2 : [5] a supprimé Authors 05/01/2022 15:57:00



Page 2 : [5] a supprimé Authors 05/01/2022 15:57:00



Page 2 : [5] a supprimé Authors 05/01/2022 15:57:00



Page 2 : [6] a supprimé Authors 05/01/2022 15:57:00



Page 2 : [6] a supprimé Authors 05/01/2022 15:57:00



Page 2 : [7] a supprimé Authors 05/01/2022 15:57:00



Page 2 : [7] a supprimé Authors 05/01/2022 15:57:00



Page 2 : [8] a supprimé Authors 05/01/2022 15:57:00



Page 2 : [9] a supprimé Authors 05/01/2022 15:57:00



Page 2 : [10] a supprimé Authors 05/01/2022 15:57:00



Page 2 : [10] a supprimé Authors 05/01/2022 15:57:00



Page 2 : [10] a supprimé Authors 05/01/2022 15:57:00



Page 3 : [11] a supprimé Authors 05/01/2022 15:57:00



Page 3 : [12] a supprimé Authors 05/01/2022 15:57:00



Page 3 : [13] a supprimé Authors 05/01/2022 15:57:00



Page 3 : [14] a supprimé Authors 05/01/2022 15:57:00



Page 3 : [15] a supprimé Authors 05/01/2022 15:57:00



Page 3 : [16] a supprimé Authors 05/01/2022 15:57:00



Page 4 : [17] a supprimé Authors 05/01/2022 15:57:00



Page 4 : [17] a supprimé Authors 05/01/2022 15:57:00



Page 4 : [18] a supprimé Authors 05/01/2022 15:57:00



Page 4 : [18] a supprimé Authors 05/01/2022 15:57:00



Page 4 : [18] a supprimé Authors 05/01/2022 15:57:00



Page 4 : [18] a supprimé Authors 05/01/2022 15:57:00



Page 4 : [18] a supprimé Authors 05/01/2022 15:57:00



Page 4 : [18] a supprimé Authors 05/01/2022 15:57:00



Page 4 : [18] a supprimé Authors 05/01/2022 15:57:00



Page 4 : [18] a supprimé Authors 05/01/2022 15:57:00



Page 4 : [18] a supprimé Authors 05/01/2022 15:57:00



Page 4 : [18] a supprimé Authors 05/01/2022 15:57:00



Page 4 : [18] a supprimé Authors 05/01/2022 15:57:00



Page 4 : [18] a supprimé Authors 05/01/2022 15:57:00



Page 4 : [18] a supprimé Authors 05/01/2022 15:57:00



Page 4 : [18] a supprimé Authors 05/01/2022 15:57:00



Page 4 : [18] a supprimé Authors 05/01/2022 15:57:00



Page 4 : [18] a supprimé Authors 05/01/2022 15:57:00



Page 4 : [18] a supprimé Authors 05/01/2022 15:57:00



Page 4 : [18] a supprimé Authors 05/01/2022 15:57:00



Page 4 : [18] a supprimé Authors 05/01/2022 15:57:00



Page 4 : [18] a supprimé Authors 05/01/2022 15:57:00



Page 4 : [18] a supprimé Authors 05/01/2022 15:57:00



Page 4 : [18] a supprimé Authors 05/01/2022 15:57:00



Page 4 : [19] a supprimé Authors 05/01/2022 15:57:00



Page 4 : [19] a supprimé Authors 05/01/2022 15:57:00



Page 4 : [19] a supprimé Authors 05/01/2022 15:57:00



Page 4 : [19] a supprimé Authors 05/01/2022 15:57:00



Page 4 : [19] a supprimé Authors 05/01/2022 15:57:00



Page 4 : [19] a supprimé Authors 05/01/2022 15:57:00



Page 4 : [19] a supprimé Authors 05/01/2022 15:57:00



Page 4 : [19] a supprimé Authors 05/01/2022 15:57:00



Page 4 : [19] a supprimé Authors 05/01/2022 15:57:00



Page 4 : [19] a supprimé Authors 05/01/2022 15:57:00



Page 4 : [19] a supprimé Authors 05/01/2022 15:57:00



Page 4 : [19] a supprimé Authors 05/01/2022 15:57:00



Page 4 : [19] a supprimé Authors 05/01/2022 15:57:00



Page 4 : [19] a supprimé Authors 05/01/2022 15:57:00



Page 4 : [19] a supprimé Authors 05/01/2022 15:57:00



Page 4 : [20] a supprimé Authors 05/01/2022 15:57:00

Page 7 : [21] a supprimé Authors 05/01/2022 15:57:00



Page 7 : [21] a supprimé Authors 05/01/2022 15:57:00



Page 7 : [21] a supprimé Authors 05/01/2022 15:57:00



Page 7 : [21] a supprimé Authors 05/01/2022 15:57:00



Page 7 : [21] a supprimé Authors 05/01/2022 15:57:00



Page 7 : [22] a supprimé Authors 05/01/2022 15:57:00



Page 7 : [22] a supprimé Authors 05/01/2022 15:57:00



Page 7 : [22] a supprimé Authors 05/01/2022 15:57:00



Page 7 : [22] a supprimé Authors 05/01/2022 15:57:00



Page 7 : [23] a supprimé Authors 05/01/2022 15:57:00



Page 7 : [23] a supprimé Authors 05/01/2022 15:57:00



Page 7 : [23] a supprimé Authors 05/01/2022 15:57:00



Page 7 : [23] a supprimé Authors 05/01/2022 15:57:00



Page 7 : [24] a supprimé Authors 05/01/2022 15:57:00



Page 7 : [24] a supprimé Authors 05/01/2022 15:57:00



Page 7 : [24] a supprimé Authors 05/01/2022 15:57:00



Page 7 : [24] a supprimé Authors 05/01/2022 15:57:00

▼
Page 7 : [24] a supprimé Authors 05/01/2022 15:57:00

▼
Page 7 : [24] a supprimé Authors 05/01/2022 15:57:00

▼
Page 7 : [24] a supprimé Authors 05/01/2022 15:57:00

▼
Page 7 : [24] a supprimé Authors 05/01/2022 15:57:00

▼
Page 7 : [25] a supprimé Authors 05/01/2022 15:57:00

▼
Page 7 : [25] a supprimé Authors 05/01/2022 15:57:00

▼
Page 7 : [25] a supprimé Authors 05/01/2022 15:57:00

▼
Page 7 : [25] a supprimé Authors 05/01/2022 15:57:00

▼
Page 7 : [26] a supprimé Authors 05/01/2022 15:57:00

▼
Page 7 : [26] a supprimé Authors 05/01/2022 15:57:00

▼
Page 7 : [26] a supprimé Authors 05/01/2022 15:57:00

▼
Page 7 : [26] a supprimé Authors 05/01/2022 15:57:00

▼
Page 7 : [26] a supprimé Authors 05/01/2022 15:57:00

▼
Page 7 : [26] a supprimé Authors 05/01/2022 15:57:00

▼
Page 11 : [27] a supprimé Authors 05/01/2022 15:57:00

▼
Page 11 : [27] a supprimé Authors 05/01/2022 15:57:00

▼
Page 11 : [28] a supprimé Authors 05/01/2022 15:57:00

▼
Page 11 : [28] a supprimé Authors 05/01/2022 15:57:00

▼
Page 11 : [29] a supprimé Authors 05/01/2022 15:57:00

▼
Page 11 : [29] a supprimé Authors 05/01/2022 15:57:00

▼
Page 11 : [30] a supprimé Authors 05/01/2022 15:57:00

▼
Page 11 : [31] a supprimé Authors 05/01/2022 15:57:00

▼
Page 11 : [31] a supprimé Authors 05/01/2022 15:57:00

▼
Page 11 : [31] a supprimé Authors 05/01/2022 15:57:00

▼
Page 11 : [31] a supprimé Authors 05/01/2022 15:57:00

▼
Page 11 : [31] a supprimé Authors 05/01/2022 15:57:00

▼
Page 11 : [32] a supprimé Authors 05/01/2022 15:57:00

▼
Page 11 : [32] a supprimé Authors 05/01/2022 15:57:00

▼
Page 11 : [33] a supprimé Authors 05/01/2022 15:57:00

▼
Page 11 : [33] a supprimé Authors 05/01/2022 15:57:00

▼
Page 11 : [34] a supprimé Authors 05/01/2022 15:57:00

▼
Page 11 : [34] a supprimé Authors 05/01/2022 15:57:00

Page 11 : [35] a supprimé Authors 05/01/2022 15:57:00			
2 segments (South and North)	0.65 ± 0.5 (WC94) 0.8 ± 0.5 (L14)	1610 / 3383	$0.4 \pm 0.2 / 0.2 \pm 0.1$ (WC94) $0.5 \pm 0.2 / 0.2 \pm 0.1$ (L14)

Page 11 : [36] a supprimé Authors 05/01/2022 15:57:00

Page 11 : [36] a supprimé Authors 05/01/2022 15:57:00

Page 11 : [37] a supprimé Authors 05/01/2022 15:57:00

Page 11 : [37] a supprimé Authors 05/01/2022 15:57:00

Page 11 : [38] a supprimé Authors 05/01/2022 15:57:00

Page 11 : [38] a supprimé Authors 05/01/2022 15:57:00

Page 11 : [39] a supprimé Authors 05/01/2022 15:57:00

Page 11 : [39] a supprimé Authors 05/01/2022 15:57:00

Page 11 : [39] a supprimé Authors 05/01/2022 15:57:00

Page 11 : [39] a supprimé Authors 05/01/2022 15:57:00

Page 11 : [39] a supprimé Authors 05/01/2022 15:57:00

Page 11 : [39] a supprimé Authors 05/01/2022 15:57:00

Page 11 : [39] a supprimé Authors 05/01/2022 15:57:00

Page 11 : [39] a supprimé Authors 05/01/2022 15:57:00

Page 11 : [39] a supprimé Authors 05/01/2022 15:57:00

Page 11 : [39] a supprimé Authors 05/01/2022 15:57:00

Page 11 : [39] a supprimé Authors 05/01/2022 15:57:00

Page 11 : [39] a supprimé Authors 05/01/2022 15:57:00

Page 21 : [40] a supprimé Authors 05/01/2022 15:57:00

Page 21 : [41] a supprimé Authors 05/01/2022 15:57:00

Page 25 : [42] a supprimé Authors 05/01/2022 15:57:00

Page 25 : [43] a supprimé Authors 05/01/2022 15:57:00

Page 25 : [43] a supprimé Authors 05/01/2022 15:57:00

Page 25 : [43] a supprimé Authors 05/01/2022 15:57:00

Page 25 : [43] a supprimé Authors 05/01/2022 15:57:00

Page 25 : [43] a supprimé Authors 05/01/2022 15:57:00

Page 25 : [44] a supprimé Authors 05/01/2022 15:57:00

Page 25 : [44] a supprimé Authors 05/01/2022 15:57:00

Page 25 : [44] a supprimé Authors 05/01/2022 15:57:00

▼
Page 25 : [45] a supprimé Authors 05/01/2022 15:57:00

▼
Page 25 : [45] a supprimé Authors 05/01/2022 15:57:00

▼
Page 25 : [45] a supprimé Authors 05/01/2022 15:57:00

▼
Page 25 : [45] a supprimé Authors 05/01/2022 15:57:00

▼
Page 25 : [45] a supprimé Authors 05/01/2022 15:57:00

▼
Page 25 : [45] a supprimé Authors 05/01/2022 15:57:00

▼
Page 25 : [45] a supprimé Authors 05/01/2022 15:57:00

▼
Page 25 : [45] a supprimé Authors 05/01/2022 15:57:00

▼
Page 25 : [45] a supprimé Authors 05/01/2022 15:57:00

▼
Page 25 : [46] a supprimé Authors 05/01/2022 15:57:00

▼
Page 27 : [47] a supprimé Authors 05/01/2022 15:57:00

▼
Page 27 : [48] a supprimé Authors 05/01/2022 15:57:00